Profiling cell envelope-antibiotic interactions reveals vulnerabilities to β-lactams in a multidrug-resistant bacterium

Short title: Cell envelope-antibiotic interactions and β-lactam vulnerability

Andrew M Hogan [1], Aakash Natarajan [1], Dustin T Maydaniuk[1], Beltina Léon [2], Zayra Batun [1], Anna Motnenko [1], Armando Palacios [1], Alejandra Bosch [2], Silvia T Cardona [1,3]*

1. Department of Microbiology, University of Manitoba, Winnipeg, Manitoba, Canada
2. CINDEFI, CONICET-CCT La Plata, Facultad de Ciencias Exactas, Universidad Nacional de La Plata, La Plata, Buenos Aires, Argentina
3. Department of Medical Microbiology and Infectious Diseases, University of Manitoba, Winnipeg, Manitoba, Canada

*To whom correspondence should be addressed: Silvia.Cardona@umanitoba.ca

Keywords: Transposon mutagenesis, antibiotic combinations, β-lactam, undecaprenyl phosphate, β-lactamase, avibactam

Author Contributions

STC and AMH conceived the idea and design of the research; AMH, BL, and AP designed and constructed the randomly-barcoded transposon mutant library; AMH performed the chemogenomics experiments, analysed the sequencing data, performed targeted validation studies, and wrote and edited the manuscript; DT aided with sequencing data analysis; AN constructed CRISPRi mutants related to cefiderocol activity; AM performed the lipopolysaccharide analyses; ZB assessed β-lactam susceptibility of *B. cenocepacia* clinical isolates; STC edited the manuscript, and together with AB, supervised the work and provided financial support.

Abstract

The cell envelope of the Gram-negative *Burkholderia cepacia* complex (Bcc) presents unique restrictions to antibiotic penetration. As a consequence, Bcc species are notorious for causing recalcitrant multidrug-resistant infections in immunocompromised individuals, such as those living with cystic fibrosis. To systematically identify cell envelope-associated resistance and susceptibility determinants at the genome level, we constructed a high-density, randomly-barcoded transposon mutant library in the clinical isolate *B. cenocepacia* K56-2 and exposed it to a panel of more than twenty cell envelope-targeting antibiotics. By quantifying relative mutant fitness with BarSeq, followed by validation with CRISPR-interference, we profiled over a hundred new functional associations and identified novel mediators of antibiotic susceptibility in the Bcc cell envelope. We revealed new connections between β-lactam susceptibility, peptidoglycan synthesis, and blockages in undecaprenyl phosphate metabolism, which highlight a vulnerability in sharing this lipid intermediate. We then show that the clinically relevant synergy of the β-lactam/β-lactamase inhibitor combination ceftazidime/avibactam is primarily mediated by inhibition of the PenB carbapenemase. Importantly, we found that avibactam more strongly potentiates the activity of aztreonam and meropenem than ceftazidime in a panel of Bcc clinical isolates. Finally, we characterize for first time in the Bcc the iron and receptor-dependent activity of the novel siderophore-cephalosporin antibiotic, cefiderocol. Overall, our work has implications for antibiotic target prioritization, and for using additional combinations of β-lactam/β-lactamase inhibitors that can extend the utility of our current clinical arsenal of antibacterial therapies.

Author Summary

While the Gram-negative cell envelope is a major barrier to antibiotic action, we have an incomplete picture of how each component contributes to antibiotic resistance. To answer this question from a genome-wide perspective in a model of antibiotic-resistant bacteria, we constructed a library of randomly-barcoded transposon mutants in *Burkholderia cenocepacia* and exposed it to a panel of diverse cell envelope-targeting antibiotics. We identified individual genes and whole pathways associated with antibiotic resistance, including several novel players. Focusing on clinically relevant antibiotics, our strategy dissected how the synergy of the important β-lactam/β-lactamase inhibitor combination ceftazidime/avibactam primarily depends upon inhibition of a single β-lactamase. Additionally, we are the first to characterise the molecular basis of the antibiotic mechanism of cefiderocol in *Burkholderia*, a new and very potent siderophore-cephalosporin conjugate drug. Encouragingly, we found that cefiderocol susceptibility was greatest at physiological iron concentrations. Overall, we highlight several avenues that can be taken to enhance or develop new therapeutic strategies against *Burkholderia* infection.

Introduction

Antimicrobial resistance is a major threat to global public health. In 2019, an estimated 4.95 million deaths were associated with drug-resistant infections [1], and the toll is expected to rise in the future [2]. Gram-negative bacteria consistently top the list as priorities for antibiotic development as they are a leading cause of antibiotic-resistant infections [3].

A significant driver of antibiotic resistance in Gram-negative bacteria lies in the double membrane composition of their cell envelope. The outer membrane is an asymmetric bilayer composed of phospholipids on the inner leaflet and lipopolysaccharide (LPS), decorated with O-antigen units, on the outer leaflet. Asymmetry is maintained by the action of the Mla pathway, which transports excess phospholipids from the outer membrane back to the inner membrane [4]. Together, the inner and outer membranes have orthogonal permeability requirements: small hydrophilic compounds (generally <600 Da; [5] are able to diffuse through water-filled porins in the outer membrane, while hydrophobic compounds are able to diffuse through the inner membrane [6]. The peptidoglycan sacculus is not involved in envelope permeability *per se*, but rather performs the essential function of maintaining cell shape and structural integrity [7]. Indeed, many components of the bacterial cell envelope are essential and have no human homologue, thus are attractive targets for a variety of antibiotics. Moreover, the use of small-molecule potentiators has gained traction as a route to increase membrane permeability and the activity of other antibiotics [8].

Bacteria of the genus *Burkholderia* are notorious for their high levels of intrinsic antibiotic resistance due in part to the unique characteristics of the cell envelope [9]. Among them, the lineage known as *Burkholderia cepacia* complex (Bcc) are opportunistic pathogens that primarily infect immunocompromised individuals. Some species, such as *B. cenocepacia*, may cause a form

of pneumonia and bacteremia known as cepacia syndrome [10]. Near uniform resistance to several antibiotic classes severely limits treatment options [11,12], and eradication protocols often require weeks to months of antibiotic cocktails [13,14]. Furthermore, although new therapies are available to treat the symptoms of cystic fibrosis (e.g. CFTR modulators), there may be limited benefit in pathogen clearance [15], but this has not yet been assessed for Bcc infection.

β-lactams remain as one of the few antibiotic classes effective against Bcc species; however, rates of resistance are over 50% [12,16]. Even combination with β-lactamase inhibitors, such as tazobactam or avibactam, may not restore sensitivity in all isolates [17]. Recently, the novel siderophore-cephalosporin conjugate antibiotic, cefiderocol, was developed and shown to have potent activity against a variety of Gram-negative pathogens [18,19]. Activity was dependent on the availability of ferric iron in the growth medium and was generally not affected by β-lactamase expression [18,20]. However, there have been no studies into the mechanism and susceptibility to cefiderocol in the Bcc. Understanding the basis of various forms of β-lactam resistance and identifying new ways to increase β-lactam susceptibility is important for treating Bcc infections.

Here, we performed a genome-wide, transposon mutant screen in *B. cenocepacia* K56-2, a previous epidemic isolate and model for Bcc research, against a wide array of cell envelope-targeting antibiotics. We reasoned that transposon disruption of certain genes would create specific deficiencies in the cell envelope, thus revealing mechanisms of cell envelope-related antibiotic resistance in K56-2. We aimed to uncover chemical-genetic interactions which could be exploited to guide therapeutic approaches. Using BarSeq to quantify mutant fitness in 22 conditions [21], we generated over a hundred new functional associations that were validated by CRISPRi. Focusing on the clinically relevant antibiotics, we uncovered that hindering undecaprenyl

phosphate recycling increased β-lactam susceptibility and that the synergy of the ceftazidime/avibactam combination relies primarily on inhibition of the PenB β-lactamase. Thus, we proposed more potent combinations of avibactam with aztreonam and meropenem. Additionally, we provide the first detailed characterisation of the activity of the novel siderophore-cephalosporin conjugate antibiotic cefiderocol, in the Bcc. Overall, we demonstrate how the analysis of genome-wide antibiotic-genetic interactions can identify susceptibility determinants and antibiotic combinations that may be exploited to bolster current antibiotic therapies.

Results

Rationale for the selected antibiotics

The Gram-negative cell envelope presents both a major permeability barrier to antibiotics and a potential source of antibiotic targets. In particular, Bcc species are known for their impermeable cell envelope (~10 fold less permeable compared to *E. coli* [22,23]), which contributes to extreme resistance to membrane-disrupting detergents and multiple classes of antibiotics [24,25]. Our goal was to probe the mechanisms governing cell envelope-related resistance in *B. cenocepacia* K56-2. We therefore assembled a diverse panel of clinical and pre-clinical antibiotics targeting many aspects of cell envelope biogenesis (Figure 1 and Figure S1A-C; all abbreviations listed in Table 1). We also included three hydrophobic large scaffold antibiotics in this panel that are generally excluded by the Gram-negative cell envelope (rifampicin [RIF], erythromycin [ERY], and novobiocin [NOV]; molecular weight > 600 Da) [5,8]. We expected the large scaffold antibiotics to highlight chemical-genetic interactions in cell envelope permeability and disruptions in major cell envelope biogenesis mechanisms. In summary, we aimed to study cell envelope-associated chemical-genetic interactions and how they may be exploited to inform novel antibiotic combinations.

Table 1. Antibiotics used for genome-wide fitness profiling

Antibiotic	IC_{20-30} Concentration (µg/mL)	Target (Process)
Ampicillin (**AMP**) †	256†	PBP3/Divisome (Cell wall synthesis)
Aztreonam (**AZT**)	40	PBP3/Divisome (Cell wall synthesis)
Cefiderocol (**CFD**)	0.04	PBP3/Divisome (Cell wall synthesis)
Ceftazidime - High (**CAZ-H**)*	4	PBP3/Divisome (Cell wall synthesis)
Ceftazidime - Low (**CAZ-L**)*	1.5	PBP3/Divisome (Cell wall synthesis)
Tazobactam (**TAZ**)	50	PBP3/Divisome (Cell wall synthesis)
Cefotetan (**CTT**)	45	PBP3/Divisome (Cell wall synthesis) + PBP2/Rod complex (Cell wall synthesis)
Meropenem (**MEM**)	3.5	PBP2/Rod complex (Cell wall synthesis)
Avibactam - High (**AVI-H**)*	115	PBP2/Rod complex (Cell wall synthesis) + Diverse β-lactamases
Avibactam - Low (**AVI-L**)*	8	PBP2/Rod complex (Cell wall synthesis) + Diverse β-lactamases
Ceftazidime/Avibactam (**AVI/CAZ**)	1.5/8	PBP2/Rod complex (Cell wall synthesis) + Diverse β-lactamases + PBP3/Divisome (Cell wall synthesis)
Cycloserine (**CYC**)	150	Alr and Ddl (Cell wall precursor synthesis)
Fosfomycin (**FOS**) †	256†	MurA (Cell wall precursor synthesis)
Bacitracin (**BAC**)	375	Und-PP (Undecaprenol metabolism)
FR-900098 (**FR-9**)	85	Dxr (Undecaprenol metabolism)
CHIR-090 (**CHIR**) †	256†	LpxC (Lipid A synthesis)
PF-04753299 (**PF-04**)	0.18	LpxC (Lipid A synthesis)
Chlorhexidine (**CHX**)	1.8	Lipid membranes
Polymyxin B (**PMB**)	550	LPS and lipid membranes
Erythromycin (**ERY**)	100	Peptide exit tunnel/23S rRNA (Protein Synthesis)
Novobiocin (**NOV**)	1.1	GyrB (DNA gyrase)
Rifampicin (**RIF**)	5.5	RpoB (Transcription)

* Two concentrations of AVI and CAZ were used. A higher concentration that independently reached the IC_{20-30}, and a lower concentration the same as that used in the synergistic AVI/CAZ combination.

† IC_{20-30} could not be reached for AMP, FOS, and CHIR, so highest concentration tested was used (256µg/mL).

Shading groups antibiotics by broad target processes.

Constructing and validating a randomly-barcoded transposon mutant library

To profile genome-wide contributions to antibiotic susceptibility and resistance, we turned to transposon mutagenesis and Illumina sequencing to measure mutant abundance during antibiotic challenges. Previously, our lab has constructed transposon mutant libraries in K56-2, a multidrug-resistant ET12 epidemic lineage clinical isolate [26], to identify the essential genome [27] and characterise targets and mechanisms of action for antimicrobials [28–30]. To leverage advances in sequencing and bioinformatic capabilities, we modified our Tn*5* transposon to contain a random 20 bp barcode (Figure S1D), greatly facilitating the tracking of mutant abundance in many conditions by Illumina sequencing [21]. After linking unique barcodes to genomic insertion site (RB-TnSeq), barcodes may be simply amplified by PCR and sequenced (BarSeq) (Figure S1D).

We generated a library of ~340,000 uniquely barcoded transposon mutants in K56-2 (approximately equally divided into 10 subpools). Library statistics can be found in Table S1. The library had a median of 12 insertions per protein-coding gene and an average spacing between insertions of 18.7 bp. We found that insertion sites were more likely in low GC-content regions and genes (Figure S2), as we observed previously [27], which may be due to Tn*5* transposon insertion and DNA sequencing biases.

To ensure we could use BarSeq to accurately quantify mutant abundance, we performed a pilot experiment with known levels of mutant depletion. Quantification of mutant abundance demonstrated high replicate reproducibility and close agreement with expected levels of depletion (Figure S3A and B). Despite a ~10-fold range in barcode recovery in pools with equal mutant abundance (Figure S3A) – variation that was not due to barcode GC-content (Figure S3C) – we were able to successfully and accurately quantify barcoded mutant depletion at small scale.

Antibiotic exposure and detection of broad interactions on whole pathways and processes

The choice of antibiotic exposure conditions has important implications for the sensitivity of high-throughput experiments. Thus, to enable detection of specific mechanism-related interactions, antibiotic doses were selected to inhibit 20 – 30% of growth relative to growth without antibiotics, as measured by OD_{600} [29,31,32] (Figure S4 and Table 1). As controls for the synergistic combination of ceftazidime/avibactam (AVI/CAZ), each component was also used at the lower concentration present in the combination as well as higher concentrations that individually inhibited 20 – 30% of growth. Ampicillin (AMP), fosfomycin (FOS), and CHIR-090 (CHIR) did not attain 20% growth inhibition so each was used at the highest concentration tested (256 µg/mL).

The entire pool of ~340,000 unique mutants was inoculated in LB medium at OD_{600} 0.025 (~75 CFU/mutant) and allowed to reach early exponential phase (OD_{600} 0.15). The cultures were then exposed to antibiotics (or 1% DMSO solvent control) for 8 hours (~10 generations), after which genomic DNA was harvested and used as template for BarSeq. High-output Illumina NextSeq flow cells were used to accommodate ~500 reads/gene for each condition and replicate. Resulting barcodes were counted and matched to insertion site, then normalized to Time 0 controls and aggregated across replicates to calculate average per-gene fitness scores [21,33].

Comparison between the DMSO control and each condition revealed hundreds of broad and specific factors that contribute to antibiotic susceptibility (Figure S5). As a first look to reveal effects on whole pathways and processes, the genes significantly affecting fitness in each condition were analysed for enrichment in BioCyc pathways and GO terms (Figures S6-S8) [34–37]. For negative fitness effects, we observed an enrichment in genes in membrane lipid metabolism

pathways (Figures S6 and S8). Additionally, we found enrichment in many GO terms related to the cell envelope (Figures S7 and S8). These are, for example, “peptidoglycan metabolic process”, “integral component of the membrane”, and “periplasmic space”. Broadly, these findings are in line with expectations that cell envelope-targeting antibiotics will report on susceptibility determinants in the cell envelope.

Identifying similar hallmarks as other chemical genetics studies would serve as additional validation of our results. For example, although antibiotics act by distinct mechanisms based on their class, many also exert as metabolic perturbations and the induction of reactive oxygen species (ROS) [38,39]. We found that disruptions in genes related to purine and pyrimidine metabolism and amino acid metabolism pathways often showed reduced susceptibility to antibiotics, especially the β-lactams (Figures S6 and S8). Inactivating these genes may slightly reduce metabolic rate and nucleotide pools, both known to affect antibiotic susceptibility [40,41]. Conversely, we found that disruptions in several genes related to ROS mitigation increased antibiotic susceptibility. When genes related to polyamine and reductant metabolism pathways were disrupted, susceptibility often increased (Figure S6). This was also detected by GO term enrichment of “response to oxidative stress” and “glutathione metabolic process” (Figure S7). Glutathione and polyamines, such as putrescine, are both known to be important in *B. cenocepacia* for protection against ROS [42,43]. Together, the corroboration of several previous works and expected findings confirms the validity of our BarSeq approach to uncover detailed chemical-genetic interactions at the foundations of antibiotic action.

The Mla pathway is important for envelope integrity and resistance to multiple antibiotics

The Mla pathway functions in retrograde transport of excess phospholipids from the outer membrane to the inner membrane, thereby maintaining an asymmetric, and more impermeable, outer membrane enriched in LPS (Figure 2A) [4,44]. In *B. cenocepacia* and *B. dolosa*, defects in the Mla pathway are known to increase susceptibility to large-scaffold antibiotics and serum [45]. However, homologous defects in *E. coli* K-12 and *P. aeruginosa* PA14 were found to not alter susceptibility to a variety of antibiotics [45]. In K56-2, the Mla pathway is encoded by six genes organized in two operons, and possibly two accessory genes (K562_RS01610 and K562_RS01615) in an adjacent operon (Figure 2B) [45].

In our BarSeq experiment, genes encoding components of the Mla pathway had negative fitness scores for nearly all tested antibiotic conditions (Figures S5 and Figure 2C). Disruptions in *mlaFED*, generally resulted in greater susceptibility increases, especially for the large scaffold antibiotics (ERY, NOV, and RIF), than did disruption in *vacJ* and *mlaCB* (Figure 2C). Indeed, the average fitness score of the Mla pathway genes negatively correlated with the molecular weight of the antibiotic (Figure 2D). This indicates the Mla pathway is important for membrane permeability, as large antibiotics are ineffective against Gram-negatives with intact membranes. To support these findings, we used CRISPR-interference (CRISPRi) [46,47] to silence the *mlaFEDvacJ* and *mlaCB* operons. Silencing these genes did not result in a growth defect (Figure S9). Using an *N*-phenyl-1-naphthylamine (NPN) uptake assay [48,49], we found that both of these mutants had substantially increased outer membrane permeability than the control (Figure 2E). We next reasoned that chemical permeabilization of the membrane may also increase antibiotic susceptibility of K56-2. We found chlorhexidine (CHX), but not polymyxin B (PMB), to greatly increase outer membrane permeability (Figure S10). Consequently, in checkerboard interaction assays, CHX synergised strongly with large scaffold antibiotics and the β-lactams (Figure 2F).

Overall, our findings of broad susceptibility profiles for mutants in the Mla pathway support a unique importance of this pathway in maintaining the permeability barrier of the outer membrane in *Burkholderia*, similar to a previous report [45].

Antagonising undecaprenyl phosphate recycling causes β-lactam susceptibility, hinders growth, and affects cell morphology

Polysaccharides are important structural and functional components of bacterial cell envelopes, including exopolysaccharides, the O-antigen, peptidoglycan, and protein *O*-glycosylation. From the BarSeq data, we observed that mutants with disruptions in LPS/O-antigen synthesis (e.g. *hldD*, *wbiGH*, *ogcA*, and K562_RS30805) and protein glycosylation (e.g. *ogcABE* and *pglL*) had altered susceptibility to several β-lactam antibiotics (Figure 3A). To examine if defects in outer membrane permeability were the source of increased antibiotic susceptibility, we assessed NPN uptake of CRISPRi mutants in genes/operons highlighted by the BarSeq experiment. We found that knockdown of genes related to LPS core and O-antigen synthesis and protein glycosylation did not significantly impair outer membrane integrity (Figure 3B), except for *hldD*. Thus, increased antibiotic susceptibility is not simply due to increased antibiotic influx alone.

We next reasoned that the enhanced susceptibility of cell envelope glycan pathway mutants to β-lactam antibiotics could be due to limitations in a shared intermediate, the lipid carrier UndP (Figure 3C). As a carrier, UndP is recycled after a cleavage step removes the linked glycans. UndP intermediates are present at low levels in Gram-negative membranes (<1% of total membrane lipids) [50–52] and both *de novo* UndP synthesis and UndP recycling are essential for viability in *E. coli* [53,54]. Therefore, limiting levels of UndP intermediates has major consequences for the bacterial cell.

Two lines of evidence support a link between UndP utilization pathways, peptidoglycan synthesis, and β-lactam susceptibility. First, disruptions in O-antigen and enterobacterial common antigen pathways render morphological defects in *E. coli* and *Shigella flexneri* similar to those caused by peptidoglycan defects [55–57]. Second, inhibition of *de novo* UndP synthesis rendered *B. cenocepacia* and *E. coli* more susceptible to β-lactams [58,59]. We thus reasoned that disruptions preventing or reducing the efficiency of UndP recycling may increase susceptibility to the β-lactams, FR-9, and bacitracin (BAC) due to the connection between UndP and peptidoglycan synthesis. Supporting our hypothesis, the BarSeq experiment showed that disruption of *dbcA*, encoding a homologue of the *E. coli uptA* DedA-family UndP flippase important for UndP recycling [60], resulted in susceptibility to β-lactams, FR-9, and BAC (Figure 3A). To validate the findings of the BarSeq experiment, we assessed susceptibility of CRISPRi mutants in genes related to cell envelope glycan metabolism to AZT, CAZ, and MEM, as representatives of the β-lactams used in the BarSeq experiment. Susceptibility moderately increased upon knockdown of cytoplasmic steps in the protein *O*-glycosylation pathway (encoded by *ogcABEI*) and LPS core synthesis (encoded by *hldD* and *wabRwaaLwabQP*) (Figure 3D).

Knockdown of LPS core synthesis genes may cause an accumulation of UndP-O-antigen intermediates in the periplasm as the O-antigen cannot be ligated to a heavily truncated core, thus possibly reducing UndP recycling. To support our genetic evidence for the interactions among UndP utilisation pathways, we used the LpxC inhibitor PF-04, which prevents lipid A formation, in checkerboard assays. We reasoned that exposing cells to PF-04 may cause accumulation of UndP-O-antigen intermediates in the periplasm, similar to knockdown of core biosynthetic genes *hldD* and *wabRwaaLwabQP*. Indeed, PF-04 strongly synergised with MEM, CTT, CAZ, AZT, and the isoprenoid synthesis inhibitor FR-9 (Figure 3E). Interaction with FR-9 suggests PF-04 may

cause sequestration of UndP-linked intermediates, while the resulting stress on peptidoglycan synthesis is supported by synergism of PF-04 with the β-lactams. We argue that the observed synergy was not likely due to increased outer membrane permeability as PF-04 did not synergise with the large scaffold antibiotics ERY, NOV, or RIF.

When we silenced LPS core and *O*-glycosylation genes, we noticed that the antibiotic susceptibility profiles were very similar, regardless of the β-lactam used (Figure 3D). This may indicate an independence from which peptidoglycan synthesis complex is targeted and instead points to an interaction with UndP levels itself. If UndP sequestration causes β-lactam susceptibility by reducing flux through peptidoglycan synthesis, we expected that reducing the total amount of UndP would produce a similar effect. We then targeted *ispDF* (encoding early genes in isoprenoid/UndP synthesis) and *uppS* (also called *ispU*, encoding UndPP synthase) with CRISPRi. As *uppS* is an essential gene and repression strongly suppresses growth (Figure S9), we carefully titrated the concentration of rhamnose to suppress growth by 20-30% for further assays. Indeed, knockdown of *ispDF* and *uppS* increased susceptibility to AZT, CAZ, and MEM (Figure 4A). However, knockdown of *ispDF* moderately increased membrane permeability (Figure 3B), suggesting that the β-lactam susceptibility of that mutant may be partly due to increased antibiotic influx. In addition to genetically depleting levels of UndP, we also investigated antibiotic interactions with FR-9 and BAC. FR-9 is an inhibitor of Dxr, which catalyzes an early step in isoprenoid biosynthesis [61], while BAC binds UndPP and prevents its recycling [62] (Figure 1). FR-9 and BAC synergised with many β-lactams, in addition to with each other (Figure 4B), demonstrating that double targeting at different points within UndP metabolic pathways greatly increases the inhibitory effect. Overall, both chemical and genetic evidence supports our assertion that depletion of free UndP pools causes β-lactam susceptibility.

Lastly, to further enhance the block in UndP metabolism, we aimed to simultaneously disrupt UndP synthesis while provoking an accumulation of UndP-linked glycans. These perturbations are expected to severely reduce free UndP pools, and as UndP is an essential molecule for peptidoglycan synthesis, the resulting effects will be synthetic lethality/sickness. To that end, we first separately deleted *hldD*, an epimerase required for LPS core saccharide synthesis, and *waaL*, the O-antigen ligase, in the K56-2::dCas9 background. Mutants of each gene are expected to accumulate UndP-linked O-antigen intermediates. The lack of O-antigen decorated LPS was verified in Δ*hldD* and Δ*waaL* by silver staining LPS extracts, but only the Δ*hldD* mutant could be complemented *in trans* (Figure S11). We then targeted *ispDF* and *uppS* for CRISPRi knockdown in the Δ*hldD* and Δ*waaL* dCas9 mutants and compared the effects to the K56-2::dCas9 background. Upon induction of dCas9 with rhamnose, knockdown of *ispDF* and *uppS* resulted in a double mutant effect with a further decrease in growth (Figure 5A). Finally, we overexpressed *wbiI* (encoding an epimerase/ dehydratase required for O-antigen synthesis) and the *wzm-wzt* O-antigen transporter in the Δ*waaL* mutant (Figure 5B). We reasoned that overexpression of the *wzm-wzt* O-antigen transporter in the Δ*waaL* mutant may reduce free UndP pools by causing accumulation of periplasmic UndP-O-antigen intermediates. As expected, this mutant displayed morphological changes, such as bulging, that are indicative of defects in the peptidoglycan matrix (Figure 5C). Furthermore, this mutant was also more susceptible to AZT, CAZ, and MEM (Figure 5D).

Overall, our results support the following model: In wild-type cells, recycling is important to replenish the UndP pools available for the essential process of peptidoglycan synthesis (Figure 5E). Blockages in UndP utilisation cause sequestration of UndP-glycan intermediates, reducing

the efficiency of recycling and the levels of free UndP available for peptidoglycan synthesis. lack of UndP impaires peptidoglycan synthesis increasing susceptibility to β-lactams.

BarSeq reveals the basis for β-lactam/avibactam synergy and rationalizes new effective combinations

AVI/CAZ is a current front-line treatment for many infections caused by multidrug-resistant Gram-negative bacteria. The synergy of the combination is due to avibactam inhibiting a broad spectrum of β-lactamases that degrade ceftazidime [63,64]. Studies on *Burkholderia* β-lactamases have focused on the Ambler class A PenB carbapenemase and the Ambler class C AmpC β-lactamase, of which only PenB is inhibited by AVI [65,66]. However, K56-2 encodes a further 19 putative β-lactamase-fold proteins, and it is unknown how/if each contributes to β-lactam resistance, and which is inhibited by AVI.

In the BarSeq experiment, we saw that transposon disruption of only two β-lactamase genes, bla_{penB} and K562_RS32470 (encoding a putative metallo-β-lactamase (MBL) fold protein; Pfam 00753) increased β-lactam susceptibility (Figure 6A). Although K562_RS32470 is annotated as an MBL, the interaction with AZT make us question this assignment as AZT is a poor substrate for most MBLs [67]; however, we did not conduct further experiments to investigate this. Additionally, disruption of *penR*, the positive regulator of bla_{penB} also increased β-lactam susceptibility (Figure 6A).

We reasoned that if the targets of AVI are the β-lactamases that degrade CAZ, transposon mutants of said β-lactamases would have a fitness defect in the presence of CAZ because CAZ cannot be degraded. The same mutants would also have a fitness defect in AVI/CAZ as in either case the β-lactamase target is chemically inhibited or genetically disrupted (Figure 6B). Using the

data from our BarSeq experiment, we compared pairs of conditions involved in the AVI/CAZ combination to identify genes important for fitness in one or both constituent conditions. For all comparisons, there were more genes unique to each condition than shared between any two, highlighting strong concentration-dependent physiological effects, even for the same antibiotic (Figure S12). Pair-wise comparison revealed that bla_{PenB} was important for fitness in both CAZ only and AVI/CAZ, while K562_RS32470 was important for fitness in CAZ only (Figure S12 and 6A). None of the other 20 putative β-lactamase-fold proteins were important for fitness in any condition tested here (Supporting Data S1). Thus, our findings suggest that PenB and K562_RS32470 are the only possible candidate β-lactamase targets of AVI in K56-2.

For validation, we assessed β-lactam susceptibility of CRISPRi knockdown mutants in bla_{AmpC}, bla_{PenB} , and K562_RS32470. In the absence of antibiotics, neither were important for growth (Figure S9). Knockdown of neither bla_{AmpC} nor K562_RS32470 altered the MIC of any of the tested β-lactams (Figure 6C and Table S2). On the other hand, knockdown of bla_{PenB} resulted in marked susceptibility to AMP, TAZ, CAZ, AZT, and MEM (up to 32-fold reduction in MIC) (Figure 6C and Table S2). We reasoned that if PenB is the major β-lactamase in K56-2, then knockdown of bla_{PenB} would result in the same MIC as adding AVI. In other words, the cells would be “blind” to the addition of AVI as the primary target is already knocked down. Indeed, in the presence of AVI, there was no change in MIC upon bla_{PenB} knockdown for CAZ and MEM (Figure 6C); however, knockdown of *penB* still reduced the MIC of AZT by 2-fold, suggesting that in the absence of PenB, K562_RS32470 may have a minor contribution to AZT resistance. This pattern is also observed when we measured β-lactamase activity using the chromogenic β-lactam derivative nitrocefin (Figure 6D). Knockdown of *penB* reduced β-lactamase activity by ~90% and was further inhibited to ~98% when AVI was added. There was no effect when K562_32470 was

knocked down. Unexpectedly, knockdown of *bla*$_{AmpC}$ increased β-lactamase activity by 13-fold. Although the MIC of the *bla*$_{AmpC}$ knockdown mutant was not altered, when we re-examined the data in the context of a dose-response, growth at subinhibitory β-lactam concentrations was substantially greater (Figure S13A). As β-lactamase activity could be inhibited by AVI, albeit at very high concentrations (Figure S13B), we suggest that knockdown of *bla*$_{AmpC}$ may induce overexpression of *bla*$_{PenB}$. Taken together, our genetic and biochemical results demonstrate that in K56-2, PenB is the predominant β-lactamase responsible for degrading clinically relevant β-lactams. Our findings also demonstrate that BarSeq can be used to elucidate the mechanisms and targets of antibiotic potentiation.

The marked β-lactam susceptibility of knockdown mutants in *bla*$_{PenB}$, together with the ability of avibactam to inhibit PenA-family β-lactamases in *Burkholderia* species [68], suggested a broader applicability of AVI/AZT and AVI/MEM combinations. Thus, we assembled a panel of 41 clinical Bcc isolates (including *B. gladioli*) spanning the last two decades and representing the most commonly recovered species across Canada. Susceptibility to AZT, CAZ, and MEM was assessed with and without 8 µg/mL AVI. Among Bcc species, MIC values of the β-lactams alone varied widely: 2 – >256 µg/mL for AZT; 0.5 – 32 µg/mL for MEM; 2 – >128 µg/mL for CAZ (Table S3). Overall, potentiation by AVI was strongest for AZT and MEM (up to 64-fold MIC reduction) (Figure 7A). These trends are in line with the changes in susceptibility upon *bla*$_{PenB}$ knockdown in K56-2 (Figure 6C). Consequently, and in the context of clinical breakpoints, 24/41 of the Bcc isolates were resistant to AZT without AVI, which was reduced to 2/41 with AVI (Figure 7B). For MEM and CAZ, 9/41 and 4/41 of the Bcc isolates were resistant without AVI, respectively, and all Bcc isolates were sensitive with AVI (Figure 7B).

The activity of AZT, CAZ, and MEM was not uniformly potentiated by AVI in all Bcc isolates. Even for K56-2, in which we have demonstrated the importance of PenB, AVI does not potentiate the activity of all β-lactams or even all cephalosporins (Table S4). Moreover, even if AVI potentiated the activity of one β-lactam, it did not guarantee potentiation for the others (Table S3). Thus, although alternative β-lactamases that are not inhibited by AVI may contribute to β-lactam resistance, they likely only play minor roles in most isolates. Overall, our findings suggest that, in addition to AVI/CAZ, combinations of AVI/AZT and AVI/MEM may be valuable therapeutic options for treating Bcc infection.

Our strain panel also included isolates of other CF pathogens: *P. aeruginosa*, *Achromobacter xylosoxidans*, and *Stenotrophomonas maltophilia*. In contrast to the activity in against the Bcc isolates, there was minimal potentiation by AVI, except with highly β-lactam resistant *P. aeruginosa* and with AZT against *S. maltophilia* (Table S3). As the potentiation of AZT, CAZ, and MEM by AVI was generally weaker in CF pathogens other than the Bcc, this highlights the differences in β-lactamase arsenals and demonstrates the need to perform genome-wide investigations in each species to uncover novel resistance mechanisms. Consequently, we suggest that among CF pathogens, combinations of AVI/AZT, AVI/CAZ, and AVI/MEM may be more tailored for use against Bcc infections.

Cefiderocol uptake is via several TonB-dependent receptors and requires physiological levels of iron for activity

Cefiderocol (CFD) is a novel antibiotic with a catechol siderophore conjugated to a cephalosporin that is structurally similar to CAZ. The siderophore chelates ferric iron and enables active transport into cells by TonB-dependent receptors (TBDRs), resulting in substantially

increased potency against a variety of Gram-negative pathogens [18,69,70]. Little is known about the activity the activity of CFD in *Burkholderia* species, except for a few cases of cefiderocol use in compassionate care [71] and as part of large strain panels [19,72] .

To explore the antibiotic mechanism of CFD, we analysed our BarSeq data for chemical-genetic interactions specific to CFD activity. Broadly, interactions were enriched in pathways related to iron and heme metabolism, which was not observed for other β-lactams (Figures S6 and S7). Additionally, disruptions of β-lactamase genes bla_{PenB} and K563_RS32470 did not affect fitness in CFD (Figure 6B and 8A). However, disruptions in K562_RS04910 (encoding a TonB-related protein) and K562_RS23150 (encoding a homologue of the *P.aeruginosa* PAO1 *piuA* TBDR) reduced susceptibility to CFD (Figure 8A). Of 24 putative TBDRs encoded by K56-2, disruption of *piuA* was the only TBDR associated with significantly enhanced fitness in the rich medium conditions of the BarSeq experiment (Supporting Data S1). We confirmed the involvement of *piuA* in CFD activity with a CRISPRi knockdown, which showed reduced susceptibility to CFD (4-fold increase in MIC in CAMHB) but not to the structurally related CAZ (Figure 8B).

Iron acquisition mechanisms, such as TBDRs, are generally upregulated in low iron conditions [73]. In *P. aeruginosa,* the susceptibility to CFD increases with decreasing iron concentrations [70]. To test the effect of iron levels on susceptibility of K56-2 to CFD, we used a low iron medium (M9 salts + casamino acids [M9+CAA]) and high iron medium (CAMHB), which we found by ICP-MS to have 0.61 µM ± 0.07 µM and 6.75 µM ± 0.71 µM total iron, respectively. Contrary what was observed in *P. aeruginosas*, the MIC of CFD was 8-fold higher in M9+CAA than in CAMHB for K56-2 (Figure 8B). This trend was also seen in many Bcc clinical isolates (Table S5). Furthermore, lowering iron levels by chelation antagonised CFD in both

CAMHB and M9+CAA (Figure 8C). While we thought that changes in susceptibility between high and low iron media may be due to reduced *piuA* receptor expression, knocking down *piuA* in M9+CAA caused a further 4-fold increase in MIC (Figure 8B). Thus, unexpectedly, low levels of iron reduced the activity of CFD in K56-2 and more broadly across Bcc species.

While infection settings are generally iron-limiting [74], the sputum of individuals with severe CF is enriched in iron (62 – 125 µM compared to ~18 µM in a healthy lung)[75]. To mimic the high iron conditions of the CF sputum, we supplemented the CAMHB and M9+CAA media with $FeCl_3$. Supplementing M9+CAA with 25 µM iron resulted in 4-fold lower MIC values (Figure 8D). At very high iron concentrations (>100 µM) in CAMHB, the MIC was 4-fold higher (Figure 8D). These effects reflect the different initial iron concentrations in rich CAMHB and defined M9+CAA, where adding small amounts of iron equilibrate CFD susceptibility between CAMHB and M9+CAA. These findings are in agreement with the importance of iron for CFD susceptibility.

We then reasoned that the BarSeq experiment, which was performed in rich LB medium, may not have captured the physiological changes that occur in low iron conditions, such as altered TBDR expression. To further study the link between CFD susceptibility and cell physiology under iron limitation, we constructed a panel of CRISPRi mutants in all 24 putative TBDRs encoded in K56-2, in addition to *fur*, encoding the Fur transcriptional repressor, and the four *tonB* paralogues (Table S6 and Figure S9). We identified two other receptors, the HmuR heme receptor homologue (K562_RS30495) and a putative CntO pseudopaline receptor homologue (K562_RS10150), that upon knockdown reduced susceptibility to CFD. Additionally, knockdown of the *tonB3* homologue also susceptibility to CFD (Figure 8B). Knockdown of the *tonB1* paralogue, however, produced opposite effects, increasing susceptibility (Figure 8B). Knockdown of *fur* increased CFD

susceptibility at least 4-fold in both CAMHB and M9+CAA, suggesting that CFD receptor gene expression is repressed by Fur.

Notably, K56-2 was much more susceptible to CFD at all iron concentrations, than to the other β-lactams, even when in combination with AVI (Table S3). In addition, the Bcc clinical isolate panel showed the same trends. Of the 41 isolates, the MIC_{50} was 0.5 µg/mL and only eight (20%) were resistant to CFD (Figure 7B and Table S3), demonstrating very potent activity. Susceptibility of the Bcc isolates to CFD was generally not affected by the addition of AVI (Table S3). Overall, our findings indicate that while there might be a critical threshold of iron required for CFD activity, CFD MIC values remain well below those of other β-lactams (Table S3).

Interactive visualization of chemogenomic interactions in a web application

To ease data accessibility, we have made an interactive and visual web app accessible at https://cardonalab.shinyapps.io/bcc_interaction_viewer/. The effects of individual antibiotics can be filtered with customizable gene fitness thresholds and assessed with output tables that display known annotations separated by interactions that either increase or decrease fitness in the selected condition. Additionally, we can update this web app to hold data from future screens. We expect this user-friendly application will add value to our dataset by allowing additional data mining.

Discussion

The alarming rate of antibiotic resistance among Gram-negative organisms requires immediate attention. NGS-based assays provide scalable high-throughput approaches that can be applied to virtually any organism. Chemical-genetic interaction profiles can be created and examined to inform on antibiotic resistance and susceptibility determinants to guide rational antibiotic combinations. Here, using *B. cenocepacia* K56-2 as a model, we measured genome-wide fitness contributions in the presence of 22 antibiotic conditions primarily targeting the cell envelope. Generation of thousands of chemical-genetic interactions allowed confident assignment and validation of over a hundred new functional associations for many genes not previously associated with antibiotic susceptibility in *Burkholderia*. By screening with compounds that target the cell envelope, the majority of the identified factors play roles in cell envelope biogenesis and represent approaches to overcome antibiotic resistance.

The centrality and essentiality of UndP for cell envelope biogenesis hints at a weakness that may be exploited for antibiotic development. In *B. cenocepacia*, at least four pathways use UndP intermediates (Figure 3C, plus the 4-amino-4-deoxy-L-arabinose [Ara4N] lipid A modification), and two are essential for growth (peptidoglycan synthesis and the Ara4N modification). Our BarSeq experiment pointed to disruptions in lipid A/O-antigen synthesis and protein *O*-glycosylation causing susceptibility to β-lactams, FR-9, and/or BAC. Targeted genetic and chemical validations indicated midpoint disruptions in these pathways caused a buildup of UndP intermediates, thus reducing the free UndP available for peptidoglycan synthesis. Mutations causing accumulation of UndP-O-antigen and UndP-enterobacterial common antigen intermediates in *E. coli* [55,56] and *Shigella flexneri* [57] are known to cause substantial morphological defects from insufficient peptidoglycan synthesis. While, β-lactam susceptibility

has been observed in large-scale screens for disruptions in UndP utilisation pathways in *A. baylyi* [32], *Vibrio cholerae* [76], *P. aeruginosa* [77,78], and *E. coli* [79]; we are the first to validate these interactions with targeted genetic and chemical investigations.

An important question that remains is if targeting UndP utilisation pathways is a viable strategy for antibiotic development. Indeed, there are two documented successes: targocil and BTZ043 [80–82]. Targocil is an inhibitor of the TarG transporter for wall teichoic acid (WTA), a surface-linked glycan constructed on UndP, in *Staphylococcus aureus.* However, as the WTA pathway is non-essential, spontaneous resistance occurs relatively frequently *in vitro* (~1 in 10^6 cells) [82]. BTZ043 is an antimycobacterial that targets DprE1 in the essential cell wall arabinan biosynthesis [81]. In the related species *Corynebacterium glutamicum* [83], BTZ043 was found to inhibit growth via sequestering decaprenyl phosphate intermediates required for peptidoglycan synthesis [84]. Overall however, the outlook is not favourable for targeting UndP utilisation pathways, as suppressor mutants are commonly identified when attempting to manipulate these non-essential pathways [56,85,86]. Furthermore, while single genetic mutations in UndP utilisation pathways in *E. coli* substantially affect cell morphology [55,56], we did not see this in K56-2 (data not shown). It was only upon deleting the *waaL* O-antigen ligase and overexpressing the *wzm-wzt* O-antigen transporter that cell morphology displayed evidence of peptidoglycan defects (Figure 5C). We suggest that *Burkholderia* may be more robust to alterations in UndP levels perhaps due to higher initial abundance of UndP, as the essential Ara4N modification may otherwise place a very high burden on UndP pools. Additionally, O-antigen synthesis in *Burkholderia* may require less UndP than in *E. coli*. The Wzy-dependent pathway predominant in *E. coli* strains uses one UndP carrier for each O-antigen subunit, while the ABC transporter-dependent pathway common in *Burkholderia* (and many other species (Greenfield and Whitfield

2012)) uses a single UndP carrier to assemble the entire polymeric O-antigen. Thus, species that use the ABC transporter-dependent O-antigen pathway may be less susceptible to antibiotic inhibition of UndP utilisation pathways.

In addition to developing new antibiotics, there is also a great deal of interest in discovering potentiators (also called adjuvants) that synergise with antibiotics to substantially increase potency. The presented transposon-based screen is well-suited to identify attractive targets for new potentiators, as gene disruption/silencing can mimic the effect of gene product inhibition with a small molecule [87]. In this context, the fitness profile of the mutant in *dbcA* deserves further attention. Disruption of *dbcA* increased susceptibility to β-lactams, BAC, FR-9, CHX, and PMB (Figure 3E). DbcA, a DedA-family UndP flippase and homologue of UptA in *E. coli* [60,88], was found to be important for the Ara4N lipid A modification in *B. thailandensis* [89], and a Δ*dbcA* mutant had a colistin MIC of 8 µg/mL (compared to > 256 µg/mL in WT). The peak sputum concentration of some inhaled colistin therapies is above 300 µg/mL sputum [90], well above the inhibitory concentration for a mutant lacking DbcA. It is tempting to suggest that DbcA, and UndP recycling more broadly, may be a linchpin in both β-lactam and cationic antibiotic resistance in *Burkholderia.* Thus, inhibiting UndP recycling with a small molecule may potentiate the activity of multiple clinically available antibiotics.

The activity of β-lactams can be potentiated by β-lactamase inhibitors, such as AVI and TAZ, by protecting them from hydrolysis by β-lactamases. AVI/CAZ shows promise as a treatment for Bcc respiratory infection [91,92]; however, resistance has been identified to this combination [17]. By comparing fitness profiles of CAZ treatment in the presence or absence of AVI, we identified that the PenB serine β-lactamase and the K562_RS32470 putative metallo-β-lactamase are targets of AVI. Targeted validations then demonstrated that PenB is the predominant

β-lactamase in K56-2 and primary target of AVI. A similar transposon-based approach was recently used by the Manoil group in *A. baylyi* to show that AVI potentiates CAZ by inhibiting the GES-14 β-lactamase, while MEM is potentiated by AVI inhibition of GES-14 and OXA-23 [32]. During our follow-up experiments with PenB, we discovered that knocking down bla_{AmpC} strongly induced β-lactamase activity in K56-2 and increased growth in subinhibitory concentrations of β-lactams (Figure 6D and S13). The *B. multivorans* ATCC17616 AmpC was shown to very slowly degrade β-lactams, leading Becka et al. to propose it plays a minor role in resistance in *B. multivorans* [66]. We build on this and suggest that the *Burkholderia* AmpC may in fact play a role in peptidoglycan recycling, perhaps by degrading the muropeptide intermediates that activate PenR; however, this requires further study.

We then exploited the dependence on PenB to demonstrate that AVI strongly potentiates AZT and MEM in a panel of Bcc clinical isolates (Figure 7 and Table S3). These combinations are not commonly reported for treatment of Bcc infection and may represent alternative therapeutic approaches. AVI/AZT is reported to be most potent against species of enterobacteria that express a serine β-lactamase (which is inhibited by AVI) and a metallo-β-lactamase (which generally cannot degrade AZT) [93]. However, for treatment of CF respiratory infections, inhaled formulations of aztreonam are available that can achieve concentrations over 725 µg/g sputum with new inhaler technology [94], which is nearly 100-fold the MIC_{50} we determined for the AVI/AZT combination. AZT is also generally-well tolerated by people with allergies to other β-lactams (Romano et al. 2011). Although inhaled MEM has been used in some cases (Hewer 2012), no other β-lactams are currently licensed as inhaled formulations.

Our genome-wide view into the mechanism of action of CFD may have an impact in moving CFD forward for therapeutic uses as it is not yet indicated to treat CF infections. We

identified three receptors for CFD uptake in K56-2: PiuA (K562_RS21350), HmuR (K562_RS30495), and K562_RS10150 (putative CntO homologue). The CRISPRi mutant panel of TBDRs we constructed may be useful for screening small molecules that enter the cell via TBDRs, as recently demonstrated for thiostrepton [95] and ubonodin [96]. Promisingly, we also found that CFD activity was not affected by disruptions in the major β-lactamases (Figure 6). Additionally, in the largest screen of CFD activity in Bcc isolates to date, 85% were susceptible to CFD alone and there was little benefit of combination with AVI (Figure 7). Indeed, CFD is generally stable to β-lactamase hydrolysis; however, the NDM-1 and NDM-5 metallo-β-lactamases are linked to resistance in *Enterobacter cloacae* and *Klebsiella pneumoniae*, respectively [97,98]. An additional consideration for CFD activity is also the concentration of iron in the growth conditions. We observed that physiological iron concentrations, even elevated levels associated with chronic CF [75], are adequate for CFD activity. Furthermore, CFD activity was reduced by iron limitation from growth in a low-iron medium and from chelation, effects that we attribute to activity of the Fur ferric uptake regulator. We therefore suggest that critical iron concentration thresholds exist that reflect the interplay between the availability of free iron for CFD to bind and the cellular responses to iron levels. In summary, we demonstrate how chemogenomics can be used to functionally annotate uncharacterised genes and prioritize targets for rational antibiotic combinations to increase effectiveness of current antibiotic therapies.

Methods and Materials

Strains, medium preparation, and growth conditions

All strains used in this study are listed in Table S7. Growth at 37ºC with 230 rpm shaking in LB-Lennox medium (Difco) was used for routine strain propagation for all strains, unless otherwise specified. Cation-adjusted MHB medium (Oxoid) for susceptibility testing was prepared as per manufacturer recommendations. The M9+CAA medium used for some susceptibility tests consisted of the following: 1x M9 salts (Difco), 25 mg/L $CaCl_2$, 12.5 mg/L $MgCl_2$, 0.3% low-iron casamino acids (Fisher), and 25 mM glycerol. All plasmids used in this study are listed in Table S8. The following selective antibiotics were used: trimethoprim (Sigma; 50 µg/mL for *E. coli* and 100 µg/mL for *B. cenocepacia*), kanamycin (Fisher Scientific; 40 µg/mL for *E. coli*), gentamicin (Fisher Scientific; 50 µg/mL for *B. cenocepacia*), and tetracycline (Sigma; 20 µg/mL for *E. coli* and 100 µg/mL for *B. cenocepacia*)

Stock solutions of D-glucose (Fisher Scientific) and L-rhamnose (Sigma) were made to 20% in de-ionized water then filter sterilized. The following antibiotics were stocked in sterile de-ionized water: kanamycin sulphate (Fisher), gentamicin sulphate (Fisher), ampicillin sodium (Sigma), ceftazidime hydrate (Sigma), ceftriaxone sodium (Sigma), cefotaxime sodium (Sigma), cephalexin hydrate (Carbosynth), cefmetazole (Sigma), cefoperazone sodium (Sigma), moxalactam sodium (Sigma), polymyxin B sulphate (Sigma), colistin sulphate (GoldBio), novobiocin sodium (Sigma), and FR-900098 sodium (Toronto Research Chemicals). The following antibiotics were stocked in 100% DMSO (Fisher): aztreonam (Alfa Aesar), cefiderocol (MedKoo Biosciences), trimethoprim (TCI America), tazobactam sodium (Alfa Aesar), cefotetan sodium (Target Mol), meropenem trihydrate (MedKoo Biosciences), avibactam sodium (MedKoo Biosciences), CHIR-090 (MedKoo Biosciences), PF-04753299 (Sigma), chlorhexidine

hydrochloride (Angene China), and rifampicin (Sigma). The following antibiotics were stocked in 95% ethanol: chloramphenicol (Sigma), tetracycline hydrochloride (Sigma), and erythromycin (Sigma). D-Cycloserine (Alfa Aesar) and fosfomycin disodium (Sigma) were both stocked in sterile Dulbecco's PBS (Sigma) pH 7.2. Ciprofloxacin hydrochloride (Sigma) and bacitracin zinc (Sigma) were both stocked in sterile 0.1M HCl.

Extraction of plasmid and genomic DNA

Plasmid DNA was routinely extracted using the EZNA Plasmid DNA Mini Kit (Omega Bio-tek) and eluted in 10 mM Tris-HCl pH 8.5. Genomic DNA was isolated from *Burkholderia* with the PureLink Genomic DNA Mini Kit (Invitrogen) or by standard isopropanol precipitation and solubilized in 10 mM Tris-HCl pH 8.5.

Construction, maintenance, and transfer of plasmids

The desired inserts were amplified by PCR using Q5 high-fidelity DNA polymerase (NEB) with the high-GC buffer as per the manufacturer's protocols. See Table S9 for a list of all primers used in this study. The Monarch PCR and DNA Cleanup Kit (NEB) and Monarch DNA Gel Extraction Kit (NEB) were routinely used to purify the DNA fragments. For restriction cloning, the appropriate restriction enzymes and T4 ligase (NEB) were used according to the manufacturer's recommendations to digest then ligate the vector and insert. To prevent self-ligation, the vector was also treated with Antarctic phosphatase (NEB). For blunt-end ligation cloning, raw PCR product was mixed with T4 DNA ligase (NEB), DpnI (NEB), and T4 polynucleotide kinase (NEB) in a custom ligase buffer (132 mM Tris-HCl pH 7.5, 20 mM $MgCl_2$, 2 mM ATP, 15% PEG6000 in de-ionized water) and incubated for 30 mins at 37°C.

A previously published python script was used to design sgRNAs [99]. sgRNAs were selected to bind as close as possible to the gene start, which has been shown to result in strong silencing [99]. To mitigate the effect of off-target gene silencing, sgRNAs with a 12 bp seed region matching any other site in the genome (adjacent to a PAM site) were removed. Additionally, sgRNAs were removed if they contained any of the following features suggested to reduce silencing efficiency: 1) PAM site of ANN or TNN, 2) the sgRNA ended in GG or GA or 3) very high (>80%) GC-content. Each gene was typically targeted by two different sgRNAs within the 5' most 75 bp, and the results of the mutant that displayed the stronger phenotype were reported.

New sgRNA targeting regions were introduced into pSCB2-sgRNA by inverse PCR as previously described [46,47,100]. Briefly, the desired targeting sequence was added as a 5' extension to a primer with sequence: 5' – GTTTTAGAGCTAGAAATAGCAAGTTAAAATAAGGC – 3'. That primer was used with primer 1092 for PCR with Q5 DNA polymerase with high-GC buffer (NEB). The raw PCR product was used for blunt end ligation as above.

E. coli DH5α was used to maintain plasmids with broad-range origins of replication. *E. coli* SY327λpir$^+$ was used to maintain plasmids containing the R6Kγ origin. Plasmids were introduced into these cells by standard transformation or electroporation

Electro-competent *B. cenocepacia* K56-2 was made as per [101] with some modifications. Briefly, 5 mL of overnight culture of the appropriate strain was split into 1 mL aliquots and washed by centrifugation at 6 000 x g for 5 mins followed by resuspension in sterile, room temperature 300 mM sucrose in de-ionized water. This washing was repeated twice more and each of the aliquots were finally resuspended in 300 mM sucrose solution and used immediately.

More commonly, plasmids were introduced into Bcc species by triparental mating [29,47]. The *E. coli* donor strain, bearing the plasmid to be mobilized, the *E. coli* MM294/pRK2013 helper strain and the *Burkholderia* recipient were mated on an LB plate and incubated overnight (16-18 hours) at 37°C. Successful exconjugants were selected on LB plates containing the appropriate antibiotics with 50 µg/mL gentamicin to select against the *E. coli* donor and helper. Colonies that appeared within 48 hours at 37°C were screened by colony PCR.

Unmarked gene deletion in K56-2

Genes were deleted as per a double homologous recombination method reported previously [102,103], with some modifications. Briefly, 360 – 450 bp of the upstream and downstream regions flanking the gene(s) to be deleted were fused and ordered as a single gBlock from IDT with *Xma*I and *Xba*I restriction sites (see Table S10 for all gBlock fragments). The fragments were cloned into pGPI-SceI and transformed into *E. coli* SY327. Plasmids were confirmed by colony PCR with primers 153 and 154, then introduced into K56-2::dCas9 by triparental mating. The first recombination was confirmed by colony PCR of trimethoprim-resistant exconjugants. To promote the second recombination, pDAI-SceI-SacB [103] was introduced by triparental mating. Trimethoprim-sensitive colonies were screened by colony PCR for successful gene deletion. To cure pDAI-SceI-SacB, colonies were patched on LB (without NaCl) + 15% sucrose (Fisher). Tetracycline-sensitive colonies were again screened by colony PCR for the deletion.

Construction of the barcoded plasposon and transposon mutant library

We wished to model our approach to barcoding on a previous report from the Deutschbauer lab [21]. They constructed a 20 bp random barcode flanked by unique priming sites

(GTCGACCTGCAGCGTACG and GAGACCTCGTGGACATC). These sequences are not found in K56-2 and were thus used for our approach. Primers 964 and 965 were used for inverse PCR of our parental plasposon pRBrhaBout. The product was circularized with In-Fusion HD Cloning (Takara Bio) as per the manufacturer's protocols. The resulting plasmid, pKS1, was sequence-confirmed to contain *Bam*HI and *Nco*I restriction sites between the inverted repeat and *dhfr*. A dsDNA fragment containing 20 random bases flanked by unique priming sites [21] and *Bam*HI and *Nco*I restriction sites was ordered from IDT with the sequence: 5′-GTTCAA*CCATG***GATGTCCACGAGGTCTCT**NNNNNNNNNNNNNNNNNNNN**CGTAC GCTGCAGGTCGAC***GGATCC***ACTTA - 3′. Italics show the *Nco*I and *Bam*HI restriction sites, while bold shows the unique priming sites; note that the end of the *Nco*I site (CCATGG) overlaps by one base (G) with one of the priming sites. As the fragment is used to generate the barcoded plasposon, pRBrha-Barcode, primers 972 and 973 were designed to amplify the fragment by PCR with Q5 polymerase and high-GC buffer (NEB). The barcode fragment and pKS1 were both digested with *Nco*I and *Bam*HI and ligated with T4 DNA ligase (NEB) at a 5:1 (insert:vector) ratio (100 ng total DNA/20 µL reaction) overnight at 16°C. The ligation mix was heated inactivated at 65°C for 15 mins then 5 µL was electroporated into *E. coli* SY327 and plated on LB plates with 50 µg/mL trimethoprim. Colonies were collected in subpools of 200 000 – 600 000 and frozen in PCR tubes at -80°C until needed. This process was repeated until ~6 million donor colonies were collected. A pilot BarSeq experiment (see *2.2.7* for the method) sequenced on a MiSeq with reagent kit v2 (Génome Québec, Montréal, Canada) using the first collected subpool confirmed it was highly diverse as expected.

Each subpool of *E. coli* was used only once as donor for triparental mating with K56-2. After only 4 hours of mating at 37°C (to reduce library redundancy), the mating pellicle was spread

on Bioassay Qtrays (Molecular Devices) with the appropriate selective antibiotics and 0.2% rhamnose. After 2 days of growth, colonies were counted and harvested in subpools of 75 000 – 100 000 and frozen in PCR tubes at OD_{600} 2.0 – 4.0 (~100 million CFU/mL, or ~ 100 CFU/mutant) at -80°C. A pilot BarSeq experiment sequenced on a MiSeq with reagent kit v2 (Génome Québec, Montréal, Canada) was also performed on the first collected subpool of barcoded transposon mutants, which showed there were approximately half as many unique barcodes as total collected colonies.

RB-TnSeq DNA library preparation and sequencing

The transposon-genome junctions were amplified by the TnSeq-circle method as previously reported [27,104], with some modifications to accommodate the barcoding scheme (RB-TnSeq-circle). Briefly, DNA was extracted from representatives of the entire transposon mutant library (not treated with antibiotics) by isopropanol precipitation. The DNA was sheared with a Covaris M220 ultrasonicator, followed by end repair with the NEBNext End Repair Module (NEB). Adapters, consisting of annealed primers 683 and 684, were annealed with the Quick Ligation Kit (NEB). The DNA was then digested with *Pac*I (NEB) overnight. Probe 1426 in the presence of Ampligase (Lucigen) was used to selectively circularize and protect fragments containing the barcoded transposon sequence, while all other fragments were digested with a mix of T7 *gene 6* exonuclease (ThermoFisher), Lambda exonuclease (NEB), and Exonuclease I (NEB). qPCR with iTaq Universal SYBR Green Supermix (Bio-Rad) was used to determine enrichment of transposon-genome junctions. The number of cycles corresponding to ~50% maximum product by qPCR was used to amplify transposon-genome junctions with iTaq for Illumina sequencing. All primers used for this purpose were constructed to enable 1-step PCR to add the Illumina flow

cell adapter, Nextera index, and sequencing primer binding site. After clean-up with SeraMag beads (Cytiva), the final PCR product was first analysed on a TapeStation4150 (Agilent Technologies) then sequenced on an Illumina MiSeq (Donnelly Centre, Toronto, Canada) to assess library quality with a MiSeq reagent kit v2 (2x250 bp reads) and 20% PhiX spike. To increase sequencing depth, an Illumina HiSeq 2500 (The Applied Centre for Genomics, Toronto, Canada) was used on rapid run mode with a 20% PhiX spike (1x150bp reads). In both cases, the sequencing reads covered the transposon-specific sequence, barcode region, and at least 40 bp of the genome adjacent to the insertion site. In total, ~180 million reads were generated.

RB-TnSeq data analysis

To link barcodes to transposon insertion sites, the bioinformatic pipeline and scripts reported by Wetmore et al. [21] were used in a Conda 4.10.0 environment. These are available at https://bitbucket.org/berkeleylab/feba/src/master/. Briefly, the scripts identify reads containing the flanking priming sites and a transposon-specific sequence (terminal repeat) then map it to a genome with BLAT [105]. The priming sites flanking the barcode were the same as in the original report [21]. The transposon-specific sequence in our construct is CATGGGCACTTGTGTATAAGAGTCAG. The default stringency and base error tolerances were used, resulting in 86.1% of the observed barcodes being considered “usable” (primarily associated with one insertion site and filtered to remove sequencing/PCR errors). The reads were aligned to the closed K56-2 genome (RefSeq accession GCF_014357995.1) [106].

Transposon mutant pool antibiotic exposure

Wild-type K56-2 was used to determine the dose-response curves of the antibiotics in conditions mimicking the planned mutant pool exposure. Stationary phase cells were diluted to OD_{600} 0.025 in LB medium and grown at 37°C with 230 rpm shaking until early exponential phase (OD_{600} 0.15, about 3 hours). In 2 mL culture in glass tubes, a range of antibiotic concentrations was added (in technical duplicate) and the cells were grown for 8 hours (approximately 10-12 generations), again at 37°C with 230 rpm shaking. Then, the OD_{600} of each tube was measured to compute the dose-response curve for each antibiotic relative to cells grown without antibiotics. This assay was performed in three biological replicates. The IC_{20-30} was confirmed by repeating this assay with a much narrower antibiotic concentration range around the IC_{20-30}.

To prepare the mutant inoculum, aliquots of the transposon mutant library were thawed and mixed in ratios according to the number of colonies contained in each aliquot to obtain approximately equal abundance of each of the ~340 000 unique mutants. This master pool was then inoculated into flasks with 50 mL of LB medium with 0.2% rhamnose at OD_{600} 0.025 (~75 CFU/mutant) and grown at 37°C with 230 rpm shaking until early exponential phase (OD_{600} 0.15, about 5-6 hours from frozen stocks). The culture was then split up into 2 mL volumes in small glass tubes, six for each antibiotic: three replicate tubes at two slightly different concentrations to ensure at least one achieved the IC_{20-30}. A 2 mL aliquot of cells not exposed to antibiotic was taken as the Time 0 sample. The cultures were then exposed to antibiotics (or 1% DMSO solvent control) for 8 hours 37°C with 230 rpm shaking, after which the OD_{600} of the cultures were taken and cells were harvested from the tubes at the IC_{20-30}.

BarSeq DNA library preparation and sequencing

The method to amplify barcodes for sequencing followed a 1-step PCR as per [21] with some modifications. After antibiotic exposure, genomic DNA was extracted from cells with the PureLink Genomic DNA Mini Kit (Invitrogen). Yield for this and all subsequent steps was quantified with a Qubit (ThermoFisher) with either AccuGreen broad-range or high-sensitivity dsDNA detection kits (Biotium). To preserve mutant abundance ratios and reduce the propagation of PCR errors, semiquantitative PCR was performed. This was done for six randomly selected conditions. In each of a set of 10 µL reaction volumes, we added 40 ng of genomic DNA and 20 µM of each primer with Q5 high-fidelity DNA polymerase, the high-GC buffer, and standard Q5 reaction buffer (NEB). In an Eppendorf Mastercycler EP Gradient S, the cycling conditions were: 98°C for 4 mins, followed by cycling between 98°C for 30 s, 61°C for 30 s, 72°C for 30 s, then followed by a final extension at 72°C for 5 mins. After each cycle between 13 and 21, we quickly removed one tube and added 3 µL of Gel Loading Dye, Purple 6x (NEB) (with 10 mM EDTA) to stop the reaction. Formation of the product at 196 bp was visualized by electrophoresis through a 2.5% agarose gel in standard TAE buffer. By visual inspection of band intensities, a cycle number was chosen that resulted in ~25% of maximum product formation. This cycle number (usually 17) was the same for all six randomly selected conditions and was thus used for all conditions. These cycling conditions were found in a small pilot experiment, sequenced on a MiSeq with reagent kit v2 and 20% PhiX spike, to result in 96.4% of reads containing known barcodes.

We found that amplification profiles in 10 µL volumes matched that in 50 µL, thus the exact same PCR setup was used when scaled up to four tubes of 50 µL per condition to increase yields. For the template, 200 ng DNA was added to ensure >75 molecules of genome per mutant. We observed a minor secondary product (<10%) at 315 bp on TapeStation 4150 traces (Agilent Technologies). Thus, for each condition, 200 µL of raw BarSeq PCR product was pooled and

subjected to two rounds of dual size selection with Sera-Mag Select (Cytiva) magnetic beads to purify the desired product at 196 bp. The primers were designed with Nextera-type tagmentation sequences as for the RB-TnSeq-circle sequencing primers, except that the 8 bp standard Nextera indexes were replaced with 10 bp Unique Dual Indexes (primers 2163 – 2255, Table 3). Each product was amplified with a unique i5 and i7 index, enabling greater multiplexing flexibility and higher confidence in correcting up to 2 bp errors during indexing read sequencing. Up to 24 samples were indexed together for runs of a NextSeq 550 in high-output mode (Donnelly Centre, Toronto, Canada) with reagent kit v2.5 and 20% PhiX spike, generating 410 – 510 million 30 bp single-end reads each. A custom sequencing recipe was used for dark-cycling during the first 18 bases, covering the flanking primer region, with the read output starting at the beginning of the barcode and extending 10 bp into the other flanking priming region.

BarSeq gene fitness calculations

BarSeq reads were associated with the correct barcode using the pipeline from [21]. Reads, in fastq format, were first trimmed to contain only the 20 bp barcode using the FASTX toolkit (http://hannonlab.cshl.edu/fastx_toolkit/). Reads with any base having a quality score below 20 were also filtered out. Artificial pre- and post-sequences, NNNGTCGACCTGCAGCGTACG and AGAGACC, respectively, were added to all barcodes so the script RunBarSeq.pl would recognize the barcodes as valid.

Following this, the barcodes were processed with scripts from [33] which are designed to compare mutant abundance between conditions (https://github.com/DuttonLab/RB-TnSeq-Microbial-interactions). A pseudocount of 0.1 was added to all barcode counts to prevent 0-value errors with log transformations. Barcodes were removed if they 1) had fewer than 3 reads in the

Time 0 condition and 2) represented intergenic insertions, or insertions in the first or last 10% of a gene. Raw counts were normalized against the counts of 10 non-essential "neutral" genes randomly selected from across the genome that also showed no fitness effect in any condition. These were: K562_RS24650 (ABC-type amino acid transporter), K562_22855 (putative glycosyltransferase), K562_05000 (hydrolase family protein), K562_12100 (acyl-CoA dehydrogenase), K562_01045 (Raf kinase inhibitor-like protein), K562_06455 (putative PHA depolymerase protein), K562_13470 (GudD glucarate dehydratase), K562_16220 (DUF3025 domain-containing protein), K562_18550 (hypothetical protein), K562_28510 (hypothetical protein). Strain fitness values were then calculated as the $\log_2$(reads in Condition X / reads in Time 0). Gene fitness values were calculated as the arithmetic mean of strain fitness values for each gene. To account for artificial inflation of read count due to proximity to the replication forks, fitness values were smoothed based on genomic position using a moving window [21]. Across the three replicates, gene fitness was calculated as the inverse-variance weighted mean. Spearman, Pearson, and Lin correlation coefficients across replicates for each condition were between 0.5 and 0.8. Lastly, the gene fitness values in each condition were compared to the DMSO control by an independent two-sided Student's t-test. The data was also curated to remove any genes from downstream analysis that only had one reporting mutant. We used eggNOG-mapper v2 to provide functional annotations and gene names based on orthology [107,108].

As many bacterial genes are organized in operons, disruptions in upstream genes may have polar effects on the downstream gene expression. Consequently, observed effects would be a combination of disrupting two or more genes. We argue that polarity may have a minimal effect on our findings due to 1) high insertion density and 2) the construction of our transposon. The large number of mutants recovered in our screen virtually guarantees insertions in every non-

essential gene, thus genomic saturation would rule out polar effects by reporting fitness scores for nearly all non-essential genes. Secondly, our transposon has outward-facing promoters in both directions, the rhamnose-inducible promoter and the promoter controlling *dhfr*. As the transposon mutant antibiotic exposures were performed with added rhamnose, and the transposon terminal repeat after *dhfr* is not predicted to form an intrinsic terminator, insertion in operons may permit downstream gene expression. The parent transposon pTn*Mod*-OTp [109] was suggested to not cause polar effects [110]. However, any expression, either upstream or downstream of the insertion, would be altered/non-native but this was not directly assessed.

Microscopy

To observe the effect of deletion or overexpression of O-antigen-related genes, the appropriate mutants were inoculated in 2 mL glass tubes at OD_{600} 0.025 with or without rhamnose (0.05%) and grown at 37°C with 230 rpm shaking for 3 hours. Cells were then diluted to OD_{600} ~0.05, fixed in 3.7% formaldehyde + 1% methanol (Sigma) at room temperature for 20 minutes. The formaldehyde was quenched by addition of an equal volume of 0.5 M glycine, and the cells were washed by centrifugation and resuspended in Dulbecco's PBS (Sigma). Cells were spotted on 1.5% agarose pads with PBS to maintain turgor and imaged by DIC microscopy on an Axio Imager upright microscope (Carl Zeiss Microscopy GmbH).

LPS analysis

The general structure of the O-antigen LPS and lipid A core were analysed qualitatively by silver staining polyacrylamide gels as per [111], with some modifications. For complementation, cells were subcultured to OD_{600} 0.025 and grown for 3 hours, then induced with 0.05% rhamnose

for an additional 4 hours. For both types of mutants, an equivalent amount of 500 µL of OD_{600} 1.5 was harvested, washed by centrifugation, and resuspended in 150 µL lysis buffer (2% w/v SDS, 4% β-mercaptoethanol, 0.5 M Tris, pH 6.8). Cells were lysed by incubation at 95°C for 10 mins. DNase I (Worthington Biochemical) was added to 100 µg/mL and incubated at 37°C for 30 mins. Proteinase K (ThermoFisher) was added to 1.25 mg/mL and incubated at 60°C for 2 hr. An equal volume of 90% phenol (ThermoFisher) (supplemented with 0.1% β-mercaptoethanol and 0.2% 8-hydroxyquinoline) was added the tubes were incubated at 70°C for 15 mins, with vortexing every 5 mins. The extractions were chilled on ice for 10 mins then centrifuged at 16 000 x g for 10 mins. The aqueous phase was washed with 10x volumes of ethyl ether (saturated with 10 mM Tris and 1 mM EDTA, pH 8.0) and centrifuged briefly. The top organic phase was removed by aspiration, then the aqueous phase was gently heated to 55°C for 10 mins to boil off the remaining ethyl ether. An equivalent volume of 2x loading dye (120 mM Tris-HCl pH 6.8, 4% m/v SDS, 20% glycerol, 0.04% bromophenol blue, and 10% β-mercaptoethanol) was added and the samples were stored at -20°C until needed.

The LPS banding patterns were resolved by Tricine-SDS-PAGE as per [111], with some modifications. The gels were cast using 30% acrylamide/bis 29:1 solution (Bio-Rad) at final concentrations of 14% for the resolving gel and 4% for the stacking gel. 10 uL of each sample, diluted with an equal volume of loading buffer, was run in each lane. Gels were run at 50 V for 1 hr, then at 130 V for 3 hrs and 15 mins, then stained with the Pierce Silver Stain Kit (ThermoFisher) and imaged immediately afterwards on a Bio-Rad ChemiDoc.

Rhamnose dose-response curves

After construction, the first objective with the CRISPRi and overexpression mutants was to characterize how varying gene knockdown or overexpression affects growth. Each of the mutants were diluted to OD_{600} 0.01 in 96-well format and inoculated into fresh LB with a 2-fold rhamnose gradient (with 100 µg/mL trimethoprim). Growth was monitored in a BioTek Synergy 2 plate reader with constant linear shaking and temperature maintained at 37°C.

Antimicrobial susceptibility testing and interaction assays

Broth microdilution susceptibility tests were used to assess and interpret MIC values as per CLSI guidelines (Clinical and Laboratory Standards Institute CLSI, 2014). Overnight cultures grown in liquid LB were used to prepare inocula for standard microdilution tests and checkerboard interactions assays. Growth was visually assessed in the antibiotic gradients after 20 hrs of static incubation. When interpretive standards for *Burkholderia* did not exist (as for cefiderocol and aztreonam), standards for *Pseudomonas aeruginosa* were used.

A similar format to the standard MIC method above was used to assess changes in antibiotic susceptibility of the CRISPRi mutants. A final concentration of 0.5% rhamnose was added to the wells to induce dCas9 expression. For fitness-associated/essential genes (e.g. *uppS*), a concentration of rhamnose to achieve 80% WT growth was used. Trimethoprim was not included in the assay plates to remove the possibility of chemical interactions. Growth was assessed after 20 hrs of static incubation by reading OD_{600} values with a BioTek Synergy 2 plate reader to record subinhibitory dose effects.

Checkerboard assays were prepared in mini 4x4 well format using antibiotic concentrations of 1/8 – 1/2 the MIC for each compound. Testing was performed in cation-adjusted MHB as per CLSI guidelines. For testing with BAC, CAMHB buffered to pH 7.2 with 100 mM PBS was used

as we found the acidic solvent for BAC antagonised β-lactam susceptibility (data not shown). Checkerboard data was processed with SynergyFinder2 (http://www.synergyfinder.org/#!/) [114,115] as this easily handles biological replicates and gives mathematical interpretations of interactions even when compounds do not fully inhibit. When both the Loewe Additivity and Bliss Independence scores were below -10 (as determined from the 95% confidence intervals), the interaction was regarded as strongly antagonistic; synergy was interpreted when both scores were above +10 (as determined from the 95% confidence intervals). A weak interaction was interpreted when one score was above +10 or below -10 and the other was between -10 and +10.

Inductively coupled plasma mass spectrometry (ICP-MS) analysis of trace metals in growth media

Samples of growth medium were prepared and autoclaved as per manufacturer's recommendations. The samples were clarified by passing through a 0.22 µm PVDF syringe filter (Fisher Scientific). Bound ions were liberated by room temperature digestion 1:1 with aqua regia. The solution was then diluted 20-fold with 18.2 MΩ/cm water. ICP-MS analysis was carried out at the Ultra Clean Trace Elements Laboratory at the University of Manitoba with an Agilent 8900 ICP-QQQ-MS. The instrument plasma mode was set to general purpose with -140V omega bias and 6.6 V omega lens settings. H_2 gas flow was set to 4.5 mL/min; He gas flow was set to 4.3 mL/min; O_2 gas was set at 30%. Before the run, certified reference materials NIST-SRM 1640a and 1643e were used as a measure of quality control.

NPN uptake assay

Outer membrane permeability was assessed with the NPN uptake assay as per [48,49], with some modifications. For CRISPRi mutants, overnight cultures were grown with or without 0.5% rhamnose (or 0.04% for the *uppS* mutants) then diluted to OD_{600} 0.025 and grown for an additional 8 hours (with or without the same concentration of rhamnose) until OD_{600} ~1.0. Cells were washed by centrifugation at 5 000 x g for 5 minutes then resuspended in 5 mM HEPES pH 7.2 with 10 mM NaN_3 (Sigma) and depolarized at room temperature for 30 minutes. Then, cells were mixed with an equal volume of 5 mM HEPES buffer containing 80 µM NPN (Sigma). The fluorescence signal was measured in a BioTek Synergy 2 plate reader with filter sets: Ex 360/40 nm and Em 420/40 nm. Wild-type K56-2 treated with 32 µg/mL CHX was used as a positive permeabilized control. The blank-corrected fluorescence values were normalized to the OD_{600} of each well. To easily compare between replicates, the fluorescence ratios of the mutants to K56-2 controls (with non-targeting sgRNA as appropriate) were calculated.

Nitrocefin hydrolysis assay of β-lactamase activity

This assay was performed as per [68,116] with some modifications. Overnight cultures of the selected CRISPRi mutants were prepared with and without 0.5% rhamnose. Cultures were diluted to OD_{600} 0.1 in fresh LB with 100 µg/mL trimethoprim, both with or without 0.5% rhamnose, then grown at 37ºC with shaking until OD_{600} 2.0. Two mL of each culture were harvested, washed by centrifugation, and resuspended in lysis buffer (sodium phosphate pH 7.0, 1 mM EDTA, 40 µg/mL lysozyme). Samples of CRISPRi mutants of the putative metallo-β-lactamase K562_RS32470 were lysed without EDTA. AVI was added to half of the samples at 8 µg/mL. Cells were rested at room temperature for 30 minutes then freeze-thawed rapidly at -80ºC.

Cells were further lysed by probe sonication. The samples were clarified by centrifugation for 10 minutes at 13 000 x g at 4ºC and the supernatant was retained.

An equal volume of cell supernatant was mixed with a nitrocefin dilution in phosphate buffer pH 7.0 (final concentration of 100 µM nitrocefin (Sigma)). The absorbance at 485 nm was recorded every minute on a BioTek Synergy 2 plate reader. For each sample, the slope of the linear region of A_{485} vs. Time was calculated. The specific activity of each sample was determined by normalizing the nitrocefin hydrolysis rate by the protein concentration of each sample, as determined by a BCA assay (Pierce).

Statistical analysis

For RB-TnSeq and BarSeq data, the statistical analysis and normalizations built into the scripts were used [21,33]. Only the independent Student's t-test was applied to the BarSeq data comparisons, not the false-discovery rate multiple-testing correction as it was found to be too stringent; however, samples were only compared by t-test if they passed Fisher's F-test of equal variances ($\alpha = 0.002$). As this was expected to produce false positive, only genes with fitness effects greater than 0.5 or less than -0.5 were considered for further analysis. Additionally, we performed extensive follow-up validations using CRISPRi mutants for many of the effects we observed in the BarSeq data. Pearson's correlation with two-tailed p-values was used to assess the relationship between gene fitness values in AVI/CAZ and the single conditions in the combination. The NPN outer membrane permeability assay was analysed by 1-way ANOVA with a Dunnett's multiple comparison test, with K56-2::dCas9 bearing the non-targeting sgRNA (or without for the deletion mutants) set as the reference. β-lactamase assay data was compared by unpaired two-tailed t-tests and adjusted using Bonferroni's multiple testing correction.

Data availability

Raw sequencing data is available from the NCBI Sequencing Read Archive (SRA) under the BioProject ID PRJNA859150. All gene fitness scores are available in Supporting Data S1. Publicly available databases and servers were used for gene annotations: BioCyc (https://biocyc.org/), EggNOG-mapper v2 (http://eggnog-mapper.embl.de/), GO (http://geneontology.org/), and UniProt (https://www.uniprot.org/).

Acknowledgments

This work was financially supported by a Discovery Grant from the Natural Sciences and Engineering Research Council of Canada (NSERC), a Basic Research Grant from Cystic Fibrosis Canada, and a Research Project Grant from the Canadian Institutes of Health Research (CIHR) to STC; AMH was supported by a Vanier Canada Graduate Scholarship from CIHR; AN was supported by an Undergraduate Summer Research Award from NSERC; BL and AB were supported by the Fondo para la Investigación Científica y Tecnológica (FONCyT) Proyecto de Investigación Trianual PICT-2019-III-A, Categoría Raíces.

The authors are grateful Debbie Armstrong and Dr. Feiyue Wang from the Ultra-Clean Trace Elements Laboratory (UCTEL) at the Centre for Earth Observation Science at the University of Manitoba for ICP-MS analysis. The authors are appreciative of insightful discussions with Dr. Krisztina Papp-Wallace (Veterans Affairs Northeast Ohio Healthcare System and Case Western Reserve University) regarding the pathways and biochemistry of peptidoglycan recycling. The authors also wish to thank the Donnelly Centre (Toronto, Ontario, Canada), The Centre for Applied Genomics (Toronto, Ontario, Canada), and Génome Québec (Montréal, Québec, Canada) for sequencing services.

Conflict of Interest Statement

The authors declare no conflict of interest.

REFERENCES

1. Murray CJ, Ikuta KS, Sharara F, Swetschinski L, Aguilar GR, Gray A, et al. Global burden of bacterial antimicrobial resistance in 2019: a systematic analysis. Lancet. 2022;399: 629–655. doi:10.1016/S0140-6736(21)02724-0

2. O'Neill J. Antimicrobial Resistance: Tackling a crisis for the health and wealth of nations. The Review on Antimicrobial Resistance; 2014 Dec p. 20. Available: https://amr-review.org/sites/default/files/160525_Final%20paper_with%20cover.pdf

3. Arzanlou M, Chai WC, Venter H. Intrinsic, adaptive and acquired antimicrobial resistance in Gram-negative bacteria. Essays Biochem. 2017;61: 49–59. doi:10.1042/EBC20160063

4. Powers MJ, Simpson BW, Trent MS. The Mla pathway in *Acinetobacter baumannii* has no demonstrable role in anterograde lipid transport. eLife. 2020;9: e56571. doi:10.7554/eLife.56571

5. Decad GM, Nikaido H. Outer membrane of gram-negative bacteria. XII. Molecular-sieving function of cell wall. J Bacteriol. 1976;128: 325–336. doi:10.1128/jb.128.1.325-336.1976

6. Masi M, Réfregiers M, Pos KM, Pagès J-M. Mechanisms of envelope permeability and antibiotic influx and efflux in Gram-negative bacteria. Nat Microbiol. 2017;2: 17001. doi:10.1038/nmicrobiol.2017.1

7. van Teeseling MCF, de Pedro MA, Cava F. Determinants of bacterial morphology: from fundamentals to possibilities for antimicrobial targeting. Front Microbiol. 2017;8. Available: https://www.frontiersin.org/article/10.3389/fmicb.2017.01264

8. Klobucar K, Brown ED. New potentiators of ineffective antibiotics: Targeting the Gram-negative outer membrane to overcome intrinsic resistance. Curr Opin Chem Biol. 2022;66: 102099. doi:10.1016/j.cbpa.2021.102099

9. Rhodes KA, Schweizer HP. Antibiotic resistance in *Burkholderia* species. Drug Resist Update. 2016;28: 82–90. doi:10.1016/j.drup.2016.07.003

10. Isles A, Maclusky I, Corey M, Gold R, Prober C, Fleming P, et al. *Pseudomonas cepacia* infection in cystic fibrosis: an emerging problem. J Pediatr. 1984;104: 206–210.

11. Aaron SD, Ferris W, Henry DA, Speert DP, Macdonald NE. Multiple combination bactericidal antibiotic testing for patients with cystic fibrosis infected with *Burkholderia cepacia*. Am J Respir Crit Care Med. 2000;161: 1206–1212. doi:10.1164/ajrccm.161.4.9907147

12. Abbott FK, Milne KEN, Stead DA, Gould IM. Combination antimicrobial susceptibility testing of *Burkholderia cepacia* complex: significance of species. Int J Antimicrob Agent. 2016;48: 521–527. doi:10.1016/j.ijantimicag.2016.07.020

13. Garcia BA, Carden JL, Goodwin DL, Smith TA, Gaggar A, Leon K, et al. Implementation of a successful eradication protocol for *Burkholderia cepacia* complex in cystic fibrosis patients. BMC Pulm Med. 2018;18. doi:10.1186/s12890-018-0594-8

14. Kitt H, Lenney W, Gilchrist FJ. Two case reports of the successful eradication of new isolates of *Burkholderia cepacia* complex in children with cystic fibrosis. BMC Pharmacol Toxicol. 2016;17: 14-016-0054–0. doi:10.1186/s40360-016-0054-0 [doi]

15. Durfey SL, Pipavath S, Li A, Vo AT, Ratjen A, Carter S, et al. Combining ivacaftor and intensive antibiotics achieves limited clearance of cystic fibrosis infections. mBio. 2021; e0314821. doi:10.1128/mbio.03148-21

16. Zhou J, Chen Y, Tabibi S, Alba L, Garber E, Saiman L. Antimicrobial susceptibility and synergy studies of *Burkholderia cepacia* complex isolated from patients with cystic fibrosis. Antimicrob Agent Chemother. 2007;51: 1085–1088. doi:10.1128/AAC.00954-06

17. Everaert A, Coenye T. Effect of β-lactamase inhibitors on in vitro activity of β-lactam antibiotics against *Burkholderia cepacia* complex species. Antimicrob Resist Infect Control. 2016;5: 44. doi:10.1186/s13756-016-0142-3

18. Kohira N, West J, Ito A, Ito-Horiyama T, Nakamura R, Sato T, et al. *In vitro* antimicrobial activity of a siderophore cephalosporin, S-649266, against *Enterobacteriaceae* clinical isolates, including carbapenem-resistant strains. Antimicrob Agents Chemother. 2016;60: 729–734. doi:10.1128/AAC.01695-15

19. Hackel MA, Tsuji M, Yamano Y, Echols R, Karlowsky JA, Sahm DF. *In vitro* activity of the siderophore cephalosporin, cefiderocol, against a recent collection of clinically relevant Gram-negative bacilli from North America and Europe, including carbapenem-nonsusceptible isolates (SIDERO-WT-2014 Study). Antimicrob Agents Chemother. 2017;61: e00093-17. doi:10.1128/AAC.00093-17

20. Ito A, Nishikawa T, Matsumoto S, Yoshizawa H, Sato T, Nakamura R, et al. Siderophore cephalosporin cefiderocol utilizes ferric iron transporter systems for antibacterial activity against *Pseudomonas aeruginosa*. Antimicrob Agents Chemother. 2016;60: 7396–7401. doi:10.1128/AAC.01405-16

21. Wetmore KM, Price MN, Waters RJ, Lamson JS, He J, Hoover CA, et al. Rapid quantification of mutant fitness in diverse bacteria by sequencing randomly bar-coded transposons. mBio. 2015;6: e00306-00315. doi:10.1128/mBio.00306-15

22. Parr JT, Moore RA, Moore LV, Hancock RE. Role of porins in intrinsic antibiotic resistance of *Pseudomonas cepacia*. Antimicrob Agents Chemother. 1987;31: 121–123. doi:10.1128/AAC.31.1.121

23. Aronoff SC. Outer membrane permeability in *Pseudomonas cepacia*: diminished porin content in a beta-lactam-resistant mutant and in resistant cystic fibrosis isolates. Antimicrob Agents Chemother. 1988;32: 1636–1639. doi:10.1128/AAC.32.11.1636

24. Loutet SA, Valvano MA. Extreme antimicrobial peptide and polymyxin B resistance in the genus *Burkholderia*. Front Microbiol. 2011;2: fmicb.2011.00159. doi:10.3389/fmicb.2011.00159

25. Ahn Y, Kim JM, Kweon O, Kim S-J, Jones RC, Woodling K, et al. Intrinsic resistance of *Burkholderia cepacia* complex to benzalkonium chloride. mBio. 2016;7. doi:10.1128/mBio.01716-16

26. Darling P, Chan M, Cox AD, Sokol PA. Siderophore production by cystic fibrosis isolates of *Burkholderia cepacia*. Infect Immun. 1998;66: 874–877.

27. Gislason AS, Turner K, Domaratzki M, Cardona ST. Comparative analysis of the *Burkholderia cenocepacia* K56-2 essential genome reveals cell envelope functions that are uniquely required for survival in species of the genus *Burkholderia*. Microb Genom. 2017;3: e000140. doi:10.1099/mgen.0.000140

28. Gislason AS, Choy M, Bloodworth RAM, Qu W, Stietz MS, Li X, et al. Competitive growth enhances conditional growth mutant sensitivity to antibiotics and exposes a two-component system as an emerging antibacterial target in *Burkholderia cenocepacia*. Antimicrob Agents Chemother. 2017;61: e00790-16. doi:10.1128/AAC.00790-16

29. Hogan AM, Scoffone VC, Makarov V, Gislason AS, Tesfu H, Stietz MS, et al. Competitive fitness of essential gene knockdowns reveals a broad-spectrum antibacterial inhibitor of the cell division protein FtsZ. Antimicrob Agents Chemother. 2018;62: e01231-18. doi:10.1128/AAC.01231-18

30. Nunvar J, Hogan AM, Buroni S, Savina S, Makarov V, Cardona ST, et al. The effect of 2-thiocyanatopyridine derivative 11026103 on *Burkholderia cenocepacia*: Resistance mechanisms and systemic impact. Antibiotics. 2019;8: 159. doi:10.3390/antibiotics8040159

31. Geisinger E, Mortman NJ, Dai Y, Cokol M, Syal S, Farinha A, et al. Antibiotic susceptibility signatures identify potential antimicrobial targets in the *Acinetobacter baumannii* cell envelope. Nat Commun. 2020;11: 4522. doi:10.1038/s41467-020-18301-2

32. Bailey J, Gallagher L, Barker WT, Hubble VB, Gasper J, Melander C, et al. Genetic dissection of antibiotic adjuvant activity. mBio. 2022; e0308421. doi:10.1128/mbio.03084-21

33. Morin M, Pierce EC, Dutton RJ. Changes in the genetic requirements for microbial interactions with increasing community complexity. eLife. 2018;7: e37072. doi:10.7554/eLife.37072

34. Ashburner M, Ball CA, Blake JA, Botstein D, Butler H, Cherry JM, et al. Gene Ontology: tool for the unification of biology. Nat Genet. 2000;25: 25–29. doi:10.1038/75556

35. Castillo-Davis CI, Hartl DL. GeneMerge--post-genomic analysis, data mining, and hypothesis testing. Bioinformatics. 2003;19: 891–892. doi:10.1093/bioinformatics/btg114

36. Karp PD, Billington R, Caspi R, Fulcher CA, Latendresse M, Kothari A, et al. The BioCyc collection of microbial genomes and metabolic pathways. Brief Bioinform. 2019;20: 1085–1093. doi:10.1093/bib/bbx085

37. Gene Ontology Consortium. The Gene Ontology resource: enriching a GOld mine. Nucleic Acids Res. 2021;49: D325–D334. doi:10.1093/nar/gkaa1113

38. Kohanski MA, Dwyer DJ, Hayete B, Lawrence CA, Collins JJ. A common mechanism of cellular death induced by bactericidal antibiotics. Cell. 2007;130: 797–810. doi:10.1016/j.cell.2007.06.049

39. Dwyer DJ, Belenky PA, Yang JH, MacDonald IC, Martell JD, Takahashi N, et al. Antibiotics induce redox-related physiological alterations as part of their lethality. Proc Natl Acad Sci. 2014;111: E2100–E2109. doi:10.1073/pnas.1401876111

40. Lopatkin AJ, Stokes JM, Zheng EJ, Yang JH, Takahashi MK, You L, et al. Bacterial metabolic state more accurately predicts antibiotic lethality than growth rate. Nat Microbiol. 2019; 1–9. doi:10.1038/s41564-019-0536-0

41. Yang JH, Wright SN, Hamblin M, McCloskey D, Alcantar MA, Schrübbers L, et al. A white-box machine learning approach for revealing antibiotic mechanisms of action. Cell. 2019;177: 1649-1661.e9. doi:10.1016/j.cell.2019.04.016

42. El-Halfawy OM, Valvano MA. Putrescine reduces antibiotic-induced oxidative stress as a mechanism of modulation of antibiotic resistance in *Burkholderia cenocepacia*. Antimicrob Agents Chemother. 2014;58: 4162–4171. doi:10.1128/AAC.02649-14

43. Van Acker H, Gielis J, Acke M, Cools F, Cos P, Coenye T. The role of reactive oxygen species in antibiotic-induced cell death in *Burkholderia cepacia* complex bacteria. Kaufmann GF, editor. PLoS ONE. 2016;11: e0159837. doi:10.1371/journal.pone.0159837

44. Malinverni JC, Silhavy TJ. An ABC transport system that maintains lipid asymmetry in the gram-negative outer membrane. Proc Natl Acad Sci. 2009;106: 8009–8014. doi:10.1073/pnas.0903229106

45. Bernier SP, Son S, Surette MG. The Mla pathway plays an essential role in the intrinsic resistance of *Burkholderia cepacia* complex species to antimicrobials and host innate components. J Bacteriol. 2018;200: e00156-18. doi:10.1128/JB.00156-18

46. Qi LS, Larson MH, Gilbert LA, Doudna JA, Weissman JS, Arkin AP, et al. Repurposing CRISPR as an RNA-guided platform for sequence-specific control of gene expression. Cell. 2013;152: 1173–1183. doi:10.1016/j.cell.2013.02.022

47. Hogan AM, Rahman ASMZ, Lightly TJ, Cardona ST. A broad-host-range CRISPRi toolkit for silencing gene expression in *Burkholderia*. ACS Synth Biol. 2019;8: 2372–2384. doi:10.1021/acssynbio.9b00232

48. Loh B, Grant C, Hancock RE. Use of the fluorescent probe 1-N-phenylnaphthylamine to study the interactions of aminoglycoside antibiotics with the outer membrane of *Pseudomonas aeruginosa*. Antimicrob Agents Chemother. 1984;26: 546–551.

49. Malott RJ, Steen-Kinnaird BR, Lee TD, Speert DP. Identification of hopanoid biosynthesis genes involved in polymyxin resistance in *Burkholderia multivorans*. Antimicrob Agents Chemother. 2012;56: 464–471. doi:10.1128/AAC.00602-11

50. Trent MS, Ribeiro AA, Doerrler WT, Lin S, Cotter RJ, Raetz CR. Accumulation of a polyisoprene-linked amino sugar in polymyxin-resistant *Salmonella typhimurium* and *Escherichia coli*: Structural characterization and transfer to lipid A in the periplasm. J Biol Chem. 2001;276: 43132–43144. doi:10.1074/jbc.M106962200

51. Barreteau H, Magnet S, El Ghachi M, Touzé T, Arthur M, Mengin-Lecreulx D, et al. Quantitative high-performance liquid chromatography analysis of the pool levels of undecaprenyl phosphate and its derivatives in bacterial membranes. J Chromatogr B Analyt Technol Biomed Life Sci. 2009;877: 213–220. doi:10.1016/j.jchromb.2008.12.010

52. Wang X, Ribeiro AA, Guan Z, Raetz CRH. Identification of undecaprenyl phosphate-β-D-galactosamine in *Francisella novicida* and its function in lipid A modification. Biochemistry. 2009;48: 1162–1172. doi:10.1021/bi802211k

53. El Ghachi M, Derbise A, Bouhss A, Mengin-Lecreulx D. Identification of multiple genes encoding membrane proteins with undecaprenyl pyrophosphate phosphatase (UppP) activity in *Escherichia coli*. J Biol Chem. 2005;280: 18689–18695. doi:10.1074/jbc.M412277200

54. Baba T, Ara T, Hasegawa M, Takai Y, Okumura Y, Baba M, et al. Construction of *Escherichia coli* K-12 in-frame, single-gene knockout mutants: the Keio collection. Molecular systems biology. 2006;2: 2006.0008. doi:10.1038/msb4100050

55. Jorgenson MA, Kannan S, Laubacher ME, Young KD. Dead-end intermediates in the enterobacterial common antigen pathway induce morphological defects in *Escherichia coli* by competing for undecaprenyl phosphate. Mol Microbiol. 2016;100: mmi.13284. doi:10.1111/mmi.13284

56. Jorgenson MA, Young KD. Interrupting biosynthesis of o-antigen or the lipopolysaccharide core produces morphological defects in *Escherichia coli* by sequestering undecaprenyl phosphate. J Bacteriol. 2016;198: 3070–3079. doi:10.1128/JB.00550-16

57. Maczuga N, Tran ENH, Qin J, Morona R. Interdependence of *Shigella flexneri* O-antigen and enterobacterial common antigen biosynthetic pathways. J Bacteriol. 2022;204: e0054621. doi:10.1128/jb.00546-21

58. Sass A, Everaert A, Acker HV, Driessche FV den, Coenye T. Targeting the nonmevalonate pathway in *Burkholderia cenocepacia* increases susceptibility to certain β-

lactam antibiotics. Antimicrob Agents Chemother. 2018;62: e02607-17. doi:10.1128/AAC.02607-17

59. Jorgenson MA, MacCain WJ, Meberg BM, Kannan S, Bryant JC, Young KD. Simultaneously inhibiting undecaprenyl phosphate production and peptidoglycan synthases promotes rapid lysis in *Escherichia coli*. Mol Microbiol. 2019;112: 233–248. doi:10.1111/mmi.14265

60. Roney IJ, Rudner DZ. Two broadly conserved families of polyprenyl-phosphate transporters. Nature. 2022; 1–2. doi:10.1038/s41586-022-05587-z

61. Kuzuyama T, Shimizu T, Takahashi S, Seto H. Fosmidomycin, a specific inhibitor of 1-deoxy-d-xylulose 5-phosphate reductoisomerase in the nonmevalonate pathway for terpenoid biosynthesis. Tetra Lett. 1998;39: 7913–7916. doi:10.1016/S0040-4039(98)01755-9

62. Siewert G, Strominger JL. Bacitracin: An inhibitor of the dephosphorylation of lipid pyrophosphate, an intermediate in the biogenesis of the peptidoglycan of bacterial cell walls. Proc Natl Acad Sci. 1967;57: 767–773.

63. Ehmann DE, Jahić H, Ross PL, Gu R-F, Hu J, Kern G, et al. Avibactam is a covalent, reversible, non–β-lactam β-lactamase inhibitor. Proc Natl Acad Sci. 2012;109: 11663–11668. doi:10.1073/pnas.1205073109

64. Lahiri SD, Johnstone MR, Ross PL, McLaughlin RE, Olivier NB, Alm RA. Avibactam and class C β-lactamases: Mechanism of inhibition, conservation of the binding pocket, and implications for resistance. Antimicrob Agents Chemother. 2014;58: 5704–5713. doi:10.1128/AAC.03057-14

65. Poirel L, Rodriguez-Martinez J-M, Plésiat P, Nordmann P. Naturally occurring class A ß-lactamases from the *Burkholderia cepacia* complex. Antimicrob Agents Chemother. 2009;53: 876–882. doi:10.1128/AAC.00946-08

66. Becka SA, Zeiser ET, Barnes MD, Taracila MA, Nguyen K, Singh I, et al. Characterization of the AmpC β-lactamase from *Burkholderia multivorans*. Antimicrob Agents Chemother. 2018;62: e01140-18. doi:10.1128/AAC.01140-18

67. Felici A, Amicosante G, Oratore A, Strom R, Ledent P, Joris B, et al. An overview of the kinetic parameters of class B beta-lactamases. Biochem J. 1993;291: 151–155.

68. Zeiser ET, Becka SA, Barnes MD, Taracila MA, LiPuma JJ, Papp-Wallace KM. Resurrecting old β-lactams: potent inhibitory activity of temocillin against multidrug-resistant *Burkholderia* species isolates from the United States. Antimicrob Agent Chemother. 2019;63: e02315-18. doi:10.1128/AAC.02315-18

69. Ito A, Sato T, Ota M, Takemura M, Nishikawa T, Toba S, et al. *In vitro* antibacterial properties of cefiderocol, a novel siderophore cephalosporin, against Gram-negative bacteria. Antimicrob Agents Chemother. 2017;62. doi:10.1128/AAC.01454-17

70. Luscher A, Moynié L, Auguste PS, Bumann D, Mazza L, Pletzer D, et al. TonB-dependent receptor repertoire of *Pseudomonas aeruginosa* for uptake of siderophore-drug conjugates. Antimicrob Agent Chemother. 2018;62(6):e00097-18. doi: 10.1128/AAC.00097-18

71. Shionogi Inc. Antimicrobial drugs advisory committee: Cefiderocol briefing document. Food and Drug Administration; 2019. Available: https://www.fda.gov/media/131705/download

72. Hackel MA, Tsuji M, Yamano Y, Echols R, Karlowsky JA, Sahm DF. *In vitro* activity of the siderophore cephalosporin, cefiderocol, against carbapenem-nonsusceptible and multidrug-resistant isolates of Gram-negative bacilli collected worldwide in 2014 to 2016. Antimicrob Agents Chemother. 2018;62. doi:10.1128/AAC.01968-17

73. Butt AT, Thomas MS. Iron acquisition mechanisms and their role in the virulence of *Burkholderia* Species. Front Cell Infect Microbiol. 2017;7: 460. doi:10.3389/fcimb.2017.00460

74. Ganz T, Nemeth E. Iron homeostasis in host defence and inflammation. Nat Rev Immunol. 2015;15: 500–510. doi:10.1038/nri3863

75. Hunter RC, Asfour F, Dingemans J, Osuna BL, Samad T, Malfroot A, et al. Ferrous iron is a significant component of bioavailable iron in cystic fibrosis airways. mBio. 2013;4: e00557-13. doi:10.1128/mBio.00557-13

76. Weaver AI, Murphy SG, Umans BD, Tallavajhala S, Onyekwere I, Wittels S, et al. Genetic determinants of penicillin tolerance in *Vibrio cholerae*. Antimicrob Agents Chemother. 2018;62. doi:10.1128/AAC.01326-18

77. Dötsch A, Becker T, Pommerenke C, Magnowska Z, Jänsch L, Häussler S. Genomewide identification of genetic determinants of antimicrobial drug resistance in *Pseudomonas aeruginosa*. Antimicrob Agents Chemother. 2009;53: 2522–2531. doi:10.1128/AAC.00035-09

78. Sonnabend MS, Klein K, Beier S, Angelov A, Kluj R, Mayer C, et al. Identification of drug resistance determinants in a clinical isolate of *Pseudomonas aeruginosa* by high-density transposon mutagenesis. Antimicrob Agents Chemother. 2020;64: e01771-19. doi:10.1128/AAC.01771-19

79. Voedts H, Kennedy SP, Sezonov G, Arthur M, Hugonnet J-E. Genome-wide identification of genes required for alternative peptidoglycan cross-linking in *Escherichia coli* revealed unexpected impacts of β-lactams. Nat Commun. 2022;13: 1–14. doi:10.1038/s41467-022-35528-3

80. Lee K, Campbell J, Swoboda JG, Cuny GD, Walker S. Development of improved inhibitors of wall teichoic acid biosynthesis with potent activity against *Staphylococcus aureus*. Bioorg Med Chem Lett. 2010;20: 1767–1770. doi:10.1016/j.bmcl.2010.01.036

81. Makarov V, Manina G, Mikusova K, Mollmann U, Ryabova O, Saint-Joanis B, et al. Benzothiazinones kill *Mycobacterium tuberculosis* by blocking arabinan synthesis. Science. 2009;324: 801–804. doi:10.1126/science.1171583

82. Swoboda JG, Meredith TC, Campbell J, Brown S, Suzuki T, Bollenbach T, et al. Discovery of a small molecule that blocks wall teichoic acid biosynthesis in *Staphylococcus aureus*. ACS ChemBiol. 2009;4: 875–883. doi:10.1021/cb900151k

83. Alderwick LJ, Radmacher E, Seidel M, Gande R, Hitchen PG, Morris HR, et al. Deletion of Cg-*emb* in Corynebacterianeae leads to a novel truncated cell wall arabinogalactan, whereas inactivation of Cg-*ubiA* results in an arabinan-deficient mutant with a cell wall galactan core. J Biol Chem. 2005;280: 32362–32371. doi:10.1074/jbc.M506339200

84. Grover S, Alderwick LJ, Mishra AK, Krumbach K, Marienhagen J, Eggeling L, et al. Benzothiazinones mediate killing of Corynebacterineae by blocking decaprenyl phosphate recycling involved in cell wall biosynthesis. J Biol Chem. 2014;289: 6177–6187. doi:10.1074/jbc.M113.522623

85. Burrows LL, Lam JS. Effect of *wzx (rfbX)* mutations on A-band and B-band lipopolysaccharide biosynthesis in *Pseudomonas aeruginosa* O5. J Bacteriol. 1999;181: 973–980.

86. Xayarath B, Yother J. Mutations blocking side chain assembly, polymerization, or transport of a Wzy-dependent *Streptococcus pneumoniae* capsule are lethal in the absence of suppressor mutations and can affect polymer transfer to the cell wall. J Bacteriol. 2007;189. doi:10.1128/JB.01938-06

87. Anglada-Girotto M, Handschin G, Ortmayr K, Campos AI, Gillet L, Manfredi P, et al. Combining CRISPRi and metabolomics for functional annotation of compound libraries. Nat Chem Biol. 2022;18: 482–491. doi:10.1038/s41589-022-00970-3

88. Sit B, Srisuknimit V, Bueno E, Zingl FG, Hullahalli K, Cava F, et al. Undecaprenyl phosphate translocases confer conditional microbial fitness. Nature. 2022; 1–3. doi:10.1038/s41586-022-05569-1

89. Panta PR, Kumar S, Stafford CF, Billiot CE, Douglass MV, Herrera CM, et al. A DedA family membrane protein is required for *Burkholderia thailandensis* colistin resistance. Frontiers in Microbiology. 2019;10. Available: https://www.frontiersin.org/article/10.3389/fmicb.2019.02532

90. Yapa SWS, Li J, Patel K, Wilson JW, Dooley MJ, George J, et al. Pulmonary and systemic pharmacokinetics of inhaled and intravenous colistin methanesulfonate in cystic fibrosis patients: targeting advantage of inhalational administration. Antimicrob Agents Chemother. 2014;58: 2570–2579. doi:10.1128/AAC.01705-13

91. Papp-Wallace KM, Becka SA, Zeiser ET, Ohuchi N, Mojica MF, Gatta JA, et al. Overcoming an extremely drug resistant (XDR) pathogen: avibactam restores

susceptibility to ceftazidime for *Burkholderia cepacia* complex isolates from cystic fibrosis patients. ACS Infect Dis. 2017;3: 502–511. doi:10.1021/acsinfecdis.7b00020

92. Spoletini G, Etherington C, Shaw N, Clifton IJ, Denton M, Whitaker P, et al. Use of ceftazidime/avibactam for the treatment of MDR *Pseudomonas aeruginosa* and *Burkholderia cepacia* complex infections in cystic fibrosis: a case series. J Antimicrob Chemother. 2019;74: 1425–1429. doi:10.1093/jac/dky558

93. Biedenbach DJ, Kazmierczak K, Bouchillon SK, Sahm DF, Bradford PA. *In vitro* activity of aztreonam-avibactam against a global collection of gram-negative pathogens from 2012 and 2013. Antimicrob Agents Chemother. 2015;59: 4239–4248. doi:10.1128/AAC.00206-15

94. Gilead Sciences Inc. Cayston [package insert]. Foster City, California; 2012.

95. Ranieri MRM, Chan DCK, Yaeger LN, Rudolph M, Karabelas-Pittman S, Abdo H, et al. Thiostrepton hijacks pyoverdine receptors to inhibit growth of *Pseudomonas aeruginosa*. Antimicrob Agents Chemother. 2019;63: e00472-19. doi:10.1128/AAC.00472-19

96. Do T, Thokkadam A, Leach R, Link AJ. Phenotype-guided comparative genomics identifies the complete transport pathway of the antimicrobial lasso peptide ubonodin in *Burkholderia*. ACS Chem Biol. 2022;17: 2332–2343. doi:10.1021/acschembio.2c00420

97. Lan P, Lu Y, Chen Z, Wu X, Hua X, Jiang Y, et al. Emergence of high-level cefiderocol resistance in carbapenem-resistant *Klebsiella pneumoniae* from bloodstream infections in patients with hematologic malignancies in China. Microbiol Spectr. 2022;10: e00084-22. doi:10.1128/spectrum.00084-22

98. Nurjadi D, Kocer K, Chanthalangsy Q, Klein S, Heeg K, Boutin S. New Delhi metallo-beta-lactamase facilitates the emergence of cefiderocol resistance in *Enterobacter cloacae*. Antimicrobial Agents and Chemotherapy. 2021;66(2):e0201121. doi: 10.1128/AAC.02011-21

99. van Gestel J, Hawkins JS, Todor H, Gross CA. Computational pipeline for designing guide RNAs for mismatch-CRISPRi. STAR Protocols. 2021;2: 100521. doi:10.1016/j.xpro.2021.100521

100. Larson MH, Gilbert LA, Wang X, Lim WA, Weissman JS, Qi LS. CRISPR interference (CRISPRi) for sequence-specific control of gene expression. Nat Protoc. 2013;8: 2180–2196. doi:10.1038/nprot.2013.132

101. Choi K-H, Kumar A, Schweizer HP. A 10-min method for preparation of highly electrocompetent *Pseudomonas aeruginosa* cells: application for DNA fragment transfer between chromosomes and plasmid transformation. J Microbiol Methods. 2006;64: 391–397. doi:10.1016/j.mimet.2005.06.001

102. Flannagan RS, Linn T, Valvano MA. A system for the construction of targeted unmarked gene deletions in the genus *Burkholderia*. Environ Microbiol. 2008;10: 1652–1660. doi:10.1111/j.1462-2920.2008.01576.x

103. Hamad MA, Skeldon AM, Valvano MA. Construction of aminoglycoside-sensitive *Burkholderia cenocepacia* strains for use in studies of intracellular bacteria with the gentamicin protection assay. Appl Environ Microbiol. 2010;76: 3170–3176. doi:10.1128/AEM.03024-09

104. Gallagher LA, Shendure J, Manoil C. Genome-scale identification of resistance functions in *Pseudomonas aeruginosa* using Tn-seq. mBio. 2011;2: e00315-10. doi:10.1128/mBio.00315-10

105. Kent WJ. BLAT--the BLAST-like alignment tool. Genome Res. 2002;12: 656–664. doi:10.1101/gr.229202

106. García-Romero I, Valvano MA. Complete genome sequence of *Burkholderia cenocepacia* K56-2, an opportunistic pathogen. Microbiol Resour Announc. 2020;9. doi:10.1128/MRA.01015-20

107. Cantalapiedra CP, Hernández-Plaza A, Letunic I, Bork P, Huerta-Cepas J. eggNOG-mapper v2: Functional annotation, orthology assignments, and domain prediction at the metagenomic scale. bioRxiv. 2021; 2021.06.03.446934. doi:10.1101/2021.06.03.446934

108. Huerta-Cepas J, Forslund K, Coelho LP, Szklarczyk D, Jensen LJ, von Mering C, et al. Fast genome-wide functional annotation through orthology assignment by eggNOG-Mapper. Mol Biol Evol. 2017;34: 2115–2122. doi:10.1093/molbev/msx148

109. Hunt TA, Kooi C, Sokol PA, Valvano MA. Identification of *Burkholderia cenocepacia* genes required for bacterial survival *in vivo*. Infect Immun. 2004;72: 4010–4022.

110. Ortega X, Hunt TA, Loutet S, Vinion-Dubiel AD, Datta A, Choudhury B, et al. Reconstitution of O-specific lipopolysaccharide expression in *Burkholderia cenocepacia* strain J2315, which is associated with transmissible infections in patients with cystic fibrosis. J Bacteriol. 2005;187: 1324–1333.

111. Marolda CL, Lahiry P, Vinés E, Saldías S, Valvano MA. Micromethods for the characterization of lipid A-core and O-antigen lipopolysaccharide. Methods Mol Biol. 2006;347: 237–252. doi:10.1385/1-59745-167-3:237

112. Clinical and Laboratory Standards Institute CLSI. Methods for dilution antimicrobial susceptibility tests for bacteria that grow aerobically; approved standard—ninth edition. Pennsylvania, USA: CLSI; 2012.

113. Clinical and Laboratory Standards Institute CLSI. Performance standards for antimicrobial disk susceptibility testing; twenty-fourth informational supplement M100-S24. Wayne, PA: Clinical and Laboratory Standards Institute; 2014.

114. Ianevski A, Giri AK, Aittokallio T. SynergyFinder 2.0: visual analytics of multi-drug combination synergies. Nucleic Acids Res. 2020;48: W488–W493. doi:10.1093/nar/gkaa216

115. Zheng S, Wang W, Aldahdooh J, Malyutina A, Shadbahr T, Tanoli Z, et al. SynergyFinder Plus: Toward better interpretation and annotation of drug combination screening datasets. Genomics Proteomics Bioinformatics. 2022; S1672-0229(22)00008–0. doi:10.1016/j.gpb.2022.01.004

116. Alvarez-Ortega C, Wiegand I, Olivares J, Hancock REW, Martínez JL. Genetic determinants involved in the susceptibility of *Pseudomonas aeruginosa* to β-lactam antibiotics. Antimicrob Agents Chemother. 2010;54: 4159–4167. doi:10.1128/AAC.00257-10

Table 1. Antibiotics used for genome-wide fitness profiling

Antibiotic	IC_{20-30} Concentration (µg/mL)	Target (Process)
Ampicillin (**AMP**) †	256†	PBP3/Divisome (Cell wall synthesis)
Aztreonam (**AZT**)	40	PBP3/Divisome (Cell wall synthesis)
Cefiderocol (**CFD**)	0.04	PBP3/Divisome (Cell wall synthesis)
Ceftazidime - High (**CAZ-H**)*	4	PBP3/Divisome (Cell wall synthesis)
Ceftazidime - Low (**CAZ-L**)*	1.5	PBP3/Divisome (Cell wall synthesis)
Tazobactam (**TAZ**)	50	PBP3/Divisome (Cell wall synthesis)
Cefotetan (**CTT**)	45	PBP3/Divisome (Cell wall synthesis) + PBP2/Rod complex (Cell wall synthesis)
Meropenem (**MEM**)	3.5	PBP2/Rod complex (Cell wall synthesis)
Avibactam - High (**AVI-H**)*	115	PBP2/Rod complex (Cell wall synthesis) + Diverse β-lactamases
Avibactam - Low (**AVI-L**)*	8	PBP2/Rod complex (Cell wall synthesis) + Diverse β-lactamases
Ceftazidime/Avibactam (**AVI/CAZ**)	1.5/8	PBP2/Rod complex (Cell wall synthesis) + Diverse β-lactamases + PBP3/Divisome (Cell wall synthesis)
Cycloserine (**CYC**)	150	Alr and Ddl (Cell wall precursor synthesis)
Fosfomycin (**FOS**) †	256†	MurA (Cell wall precursor synthesis)
Bacitracin (**BAC**)	375	Und-PP (Undecaprenol metabolism)
FR-900098 (**FR-9**)	85	Dxr (Undecaprenol metabolism)
CHIR-090 (**CHIR**) †	256†	LpxC (Lipid A synthesis)
PF-04753299 (**PF-04**)	0.18	LpxC (Lipid A synthesis)
Chlorhexidine (**CHX**)	1.8	Lipid membranes
Polymyxin B (**PMB**)	550	LPS and lipid membranes
Erythromycin (**ERY**)	100	Peptide exit tunnel/23S rRNA (Protein Synthesis)
Novobiocin (**NOV**)	1.1	GyrB (DNA gyrase)
Rifampicin (**RIF**)	5.5	RpoB (Transcription)

* Two concentrations of AVI and CAZ were used. A higher concentration that independently reached the IC_{20-30}, and a lower concentration the same as that used in the synergistic AVI/CAZ combination.

† IC_{20-30} could not be reached for AMP, FOS, and CHIR, so highest concentration tested was used (256µg/mL).

Shading groups antibiotics by broad target processes.

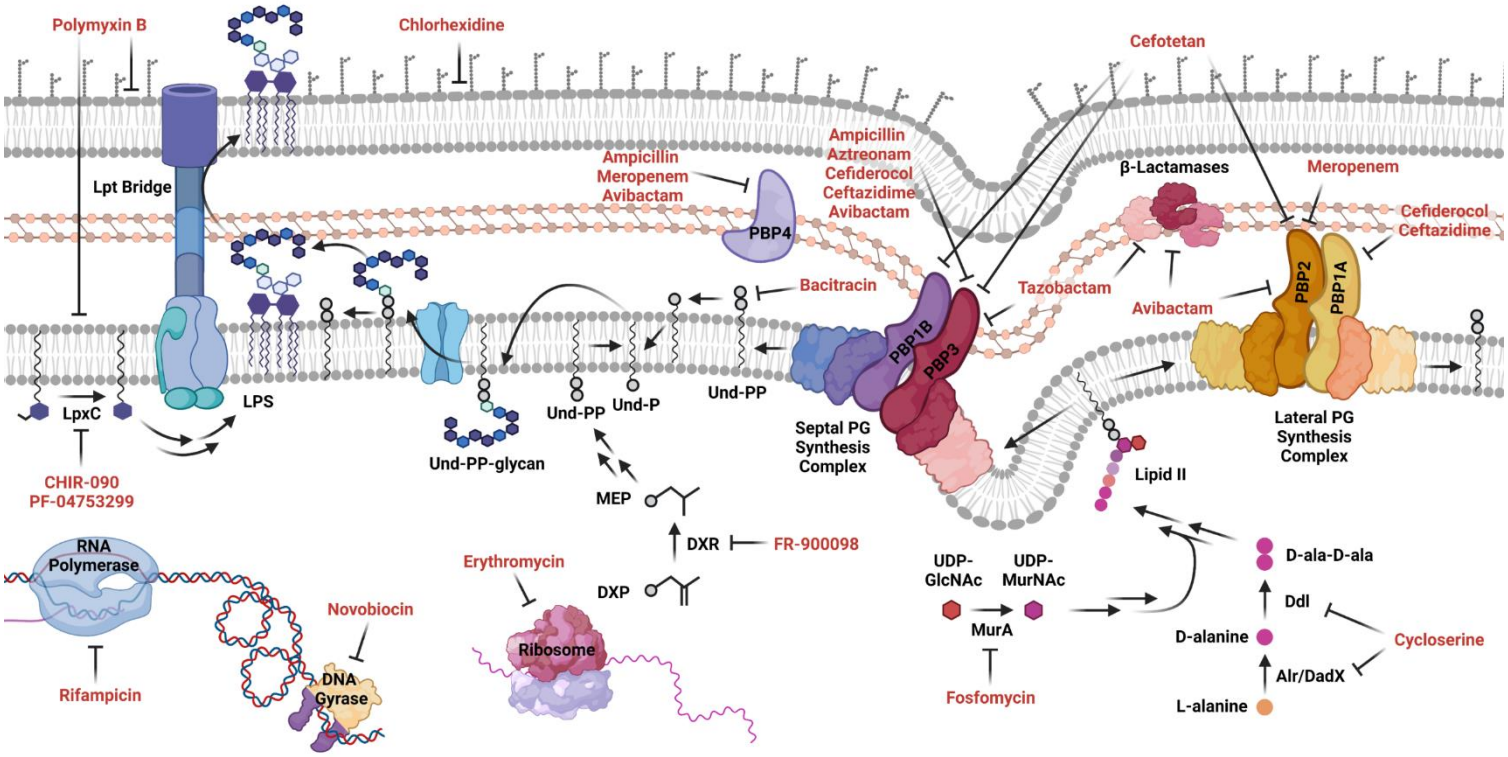

Figure 1. Schematic of the Gram-negative cell envelope and steps inhibited by the antibiotic panel. Rifampicin, novobiocin, and erythromycin are controls that do not target the envelope. Targets are shown based on previous experimental evidence from *E. coli*, and only if a Bcc homologue exists. High molecular weight PBPs 5, 6, 7 are omitted for clarity.

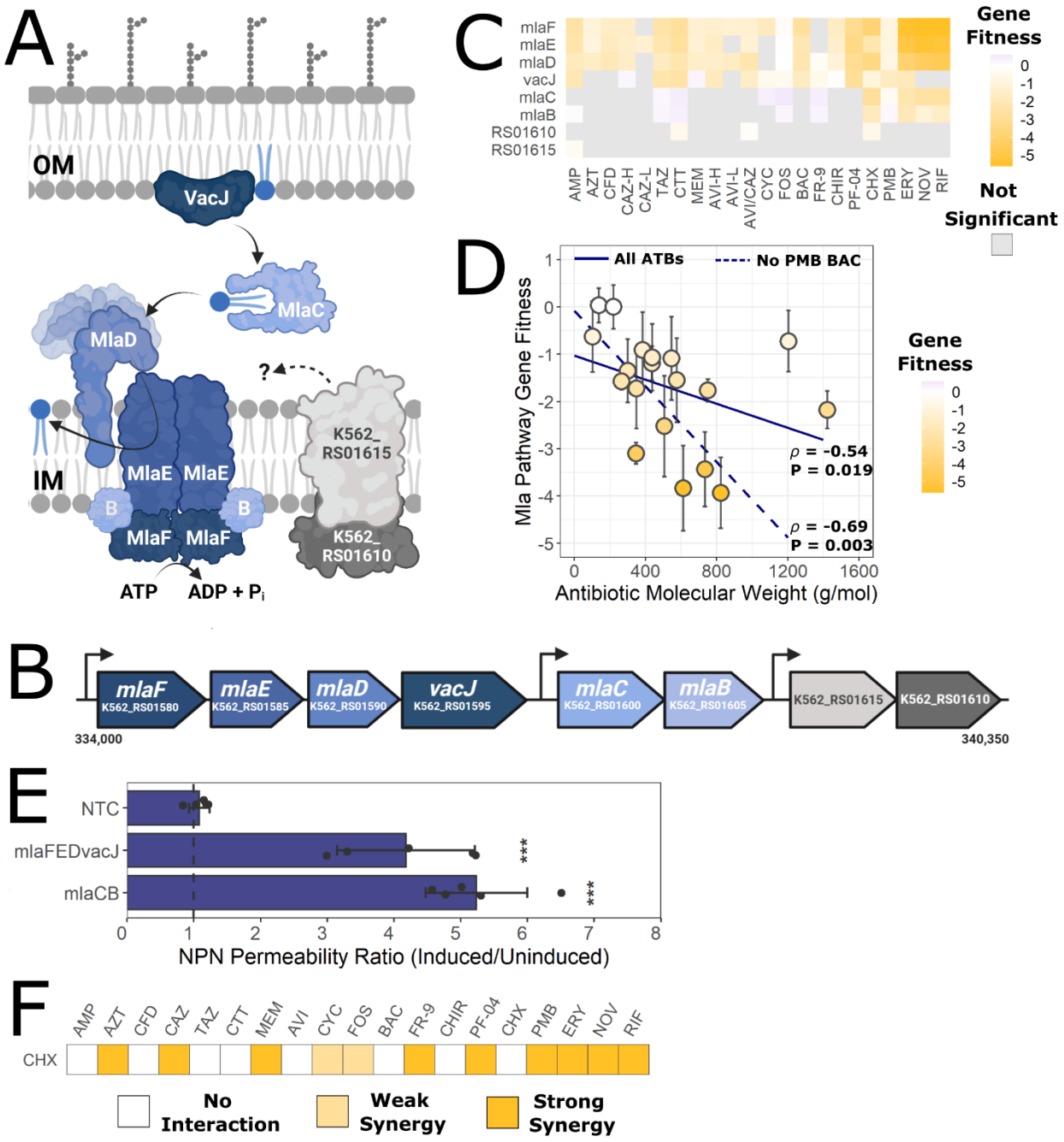

Figure 2. Defects in the Mla pathway increase susceptibility to multiple antibiotics. A) Retrograde phospholipid trafficking from the outer (OM) to inner (IM) membranes by the Mla pathway, inferred by homology [1,2]. The roles of K562_RS01610 and K562_RS01615 are unclear. B) Genetic arrangement of the Mla genes in K56-2. Nucleotide positions on chromosome 1 are noted. C) Gene fitness scores relative to DMSO control of the genes in the Mla pathway. Grey squares indicate the value was not significant (P > 0.05). D) Correlation of average gene fitness scores in the Mla pathway (*mlaFEDvacJ* and *mlaCB*) with antibiotic molecular weight. The points are coloured by average Mla pathway gene fitness score. The lines

show a linear regression with all antibiotics (solid) vs. without PMB and BAC (dashed). Shown by each line is the Spearman's rank correlation coefficient (ρ) and P-value. E) Ratios of NPN fluorescence (a measure of outer membrane permeability) of the CRISPRi mutants in inducing (0.5% rhamnose) vs uninducing (0% rhamnose) conditions. Error bars represent means ± SD of six replicates. Significance was determined by 1-way ANOVA with Dunnett's post hoc test to the wild-type control. *** $P < 0.001$. The dashed line indicates an NPN fluorescence ratio of 1. F) Summary of antibiotic checkerboard interaction assay with CHX. Interactions were assessed and interpreted with SynergyFinder as per the Materials and Methods.

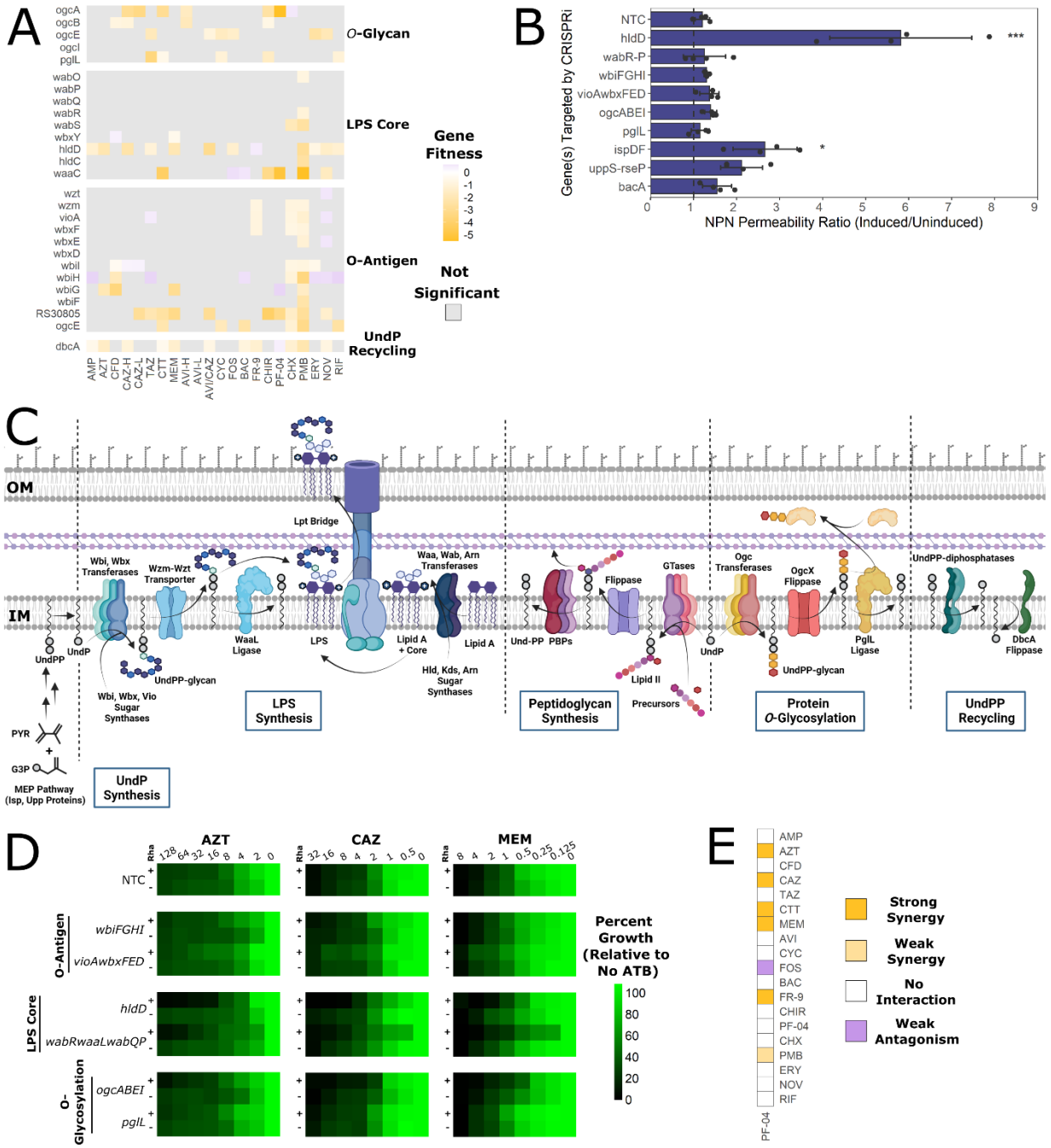

Figure 3. Defects in UndP utilisation pathways sensitize cells to β-lactams. A) Summary of the major UndP(P) metabolic pathways in B. cenocepacia (from experimental evidence and inferred by homology), annotated with proteins names if they are known [3–7]. UndPP is synthesized in the cytoplasm by the methylerythritol phosphate (MEP) pathway. UndP is a lipid carrier for construction of the O-antigen, peptidoglycan building blocks (in the form of lipid I and II), and the protein O-glycan. After use as a carrier, UndPP is liberated and recycled into UndP on the

cytoplasmic leaflet. IM = inner membrane, OM = outer membrane. B) Gene fitness scores relative to the DMSO control of the genes in the protein O-glycosylation (Ogc) pathway. C) Ratios of NPN fluorescence of the CRISPRi mutants in inducing vs uninducing conditions. Error bars represent means ± SD of four replicates. Significance was determined by 1-way ANOVA with Dunnett's post hoc test to the wild-type control. * $P < 0.05$; *** $P < 0.001$. The dashed lines indicate a NPN fluorescence ratio of 1. D) Antibiotic dose responses (µg/mL) of growth of CRISPRi mutants with or without induction with 0.5% rhamnose. Values are normalized to the OD_{600} of growth without antibiotic. NTC = non-targeting control sgRNA. E) Summary of antibiotic checkerboard interaction assay with PF-04. Interactions were assessed and interpreted with SynergyFinder as per the Materials and Methods.

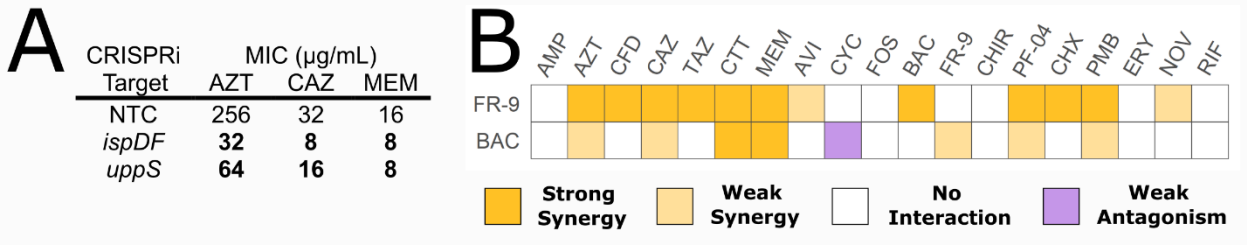

Figure 4. Inhibiting isoprenoid and UndP synthesis sensitizes cells to β-lactams. A) MIC values of K56-2::dCas9 harbouring plasmids expressing a non-targeting sgRNA control (NTC) or an sgRNA targeting the indicated genes. MIC values are medians of three biological replicates, with bold indicating at least 2-fold change from the NTC with the addition of 0.5% rhamnose. B) Summary of antibiotic checkerboard interaction assay with FR-9 and BAC. Interactions were assessed and interpreted with SynergyFinder as per the Materials and Methods.

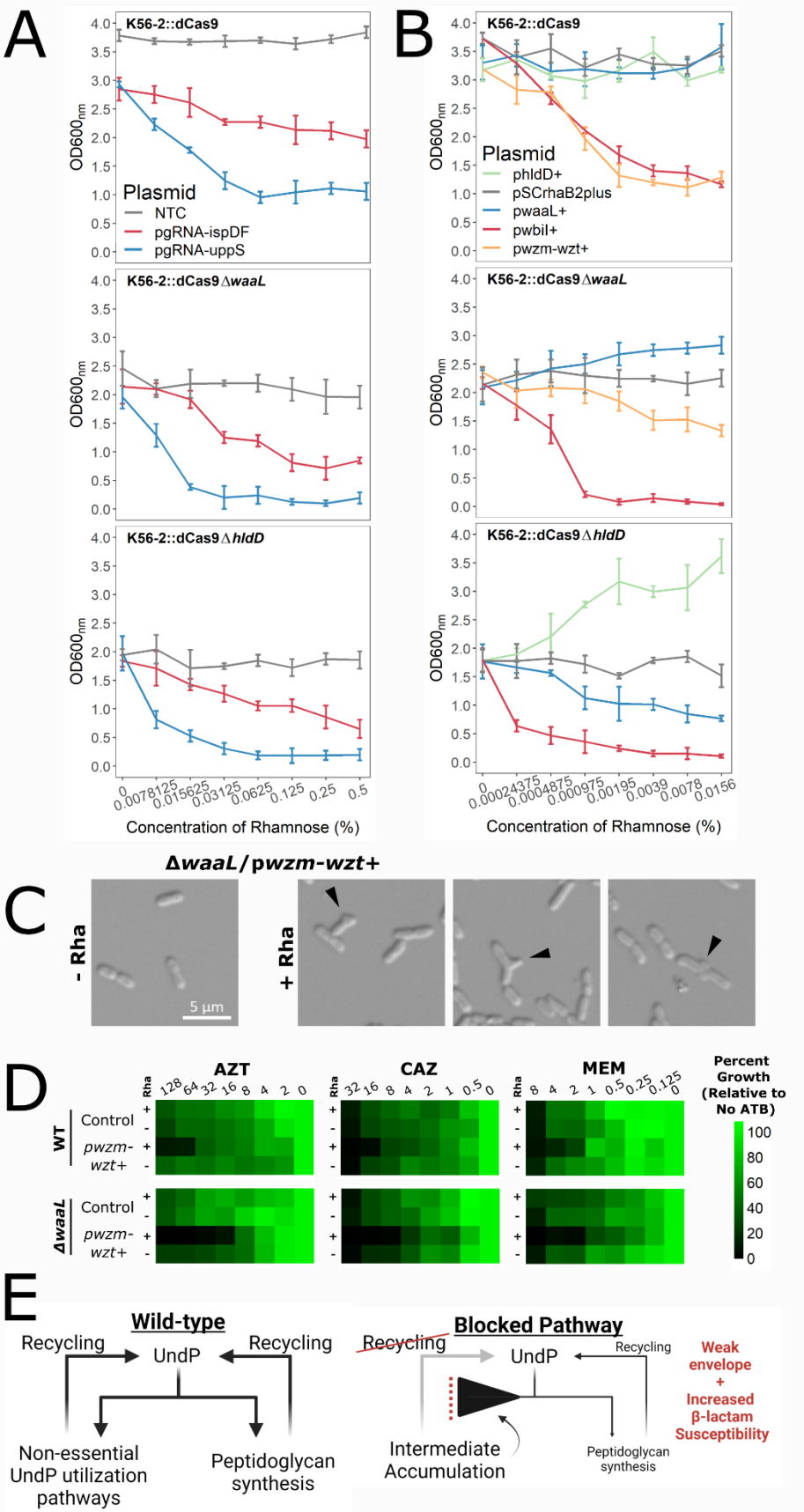
A
B
K56-2::dCas9
K56-2::dCas9 ΔwaaL
K56-2::dCas9 ΔhldD
OD600nm
Plasmid
NTC
pgRNA-ispDF
pgRNA-uppS
phldD+
pSCrhaB2plus
pwaaL+
pwbil+
pwzm-wzt+
Concentration of Rhamnose (%)
C
ΔwaaL/pwzm-wzt+
- Rha
+ Rha
5 µm
D
AZT
CAZ
MEM
Rha
Control
pwzm-wzt+
WT
ΔwaaL
Percent Growth (Relative to No ATB)
E
Wild-type
Recycling
UndP
Non-essential UndP utilization pathways
Peptidoglycan synthesis
Blocked Pathway
Intermediate Accumulation
Weak envelope + Increased β-lactam Susceptibility

Figure 5. Synthetic genetic interactions in envelope glycan metabolism link UndP sequestration to defects in the peptidoglycan matrix. Cultures of deletion mutants with A) CRISPRi plasmids or B) overexpression plasmids were grown with the indicated concentrations of rhamnose for 18 hours, the time at which the control strains reached the maximum OD_{600}. Panels are organized by mutant background: Values shown are averages of three biological replicates. C) Mid exponential phase cells of the Δ*waaL*/p*wzm-wzt*+ mutant were induced with 0.05% rhamnose for 3 hours then immobilized on 1% agarose pads and imaged by DIC at 100x magnification. The black arrowheads mark morphological abnormalities such as bulging. D) Antibiotic dose responses (µg/mL) of growth of the indicated mutants with or without induction with 0.005% rhamnose. Values are normalized to the OD_{600} of growth without antibiotic and are means of three biological replicates. Control strain harbours pSCrhaB2plus. E) Proposed framework for how disruptions in UndP metabolism reduce UndP recycling and flux into peptidoglycan synthesis, weakening the peptidoglycan matrix and increasing β-lactam susceptibility

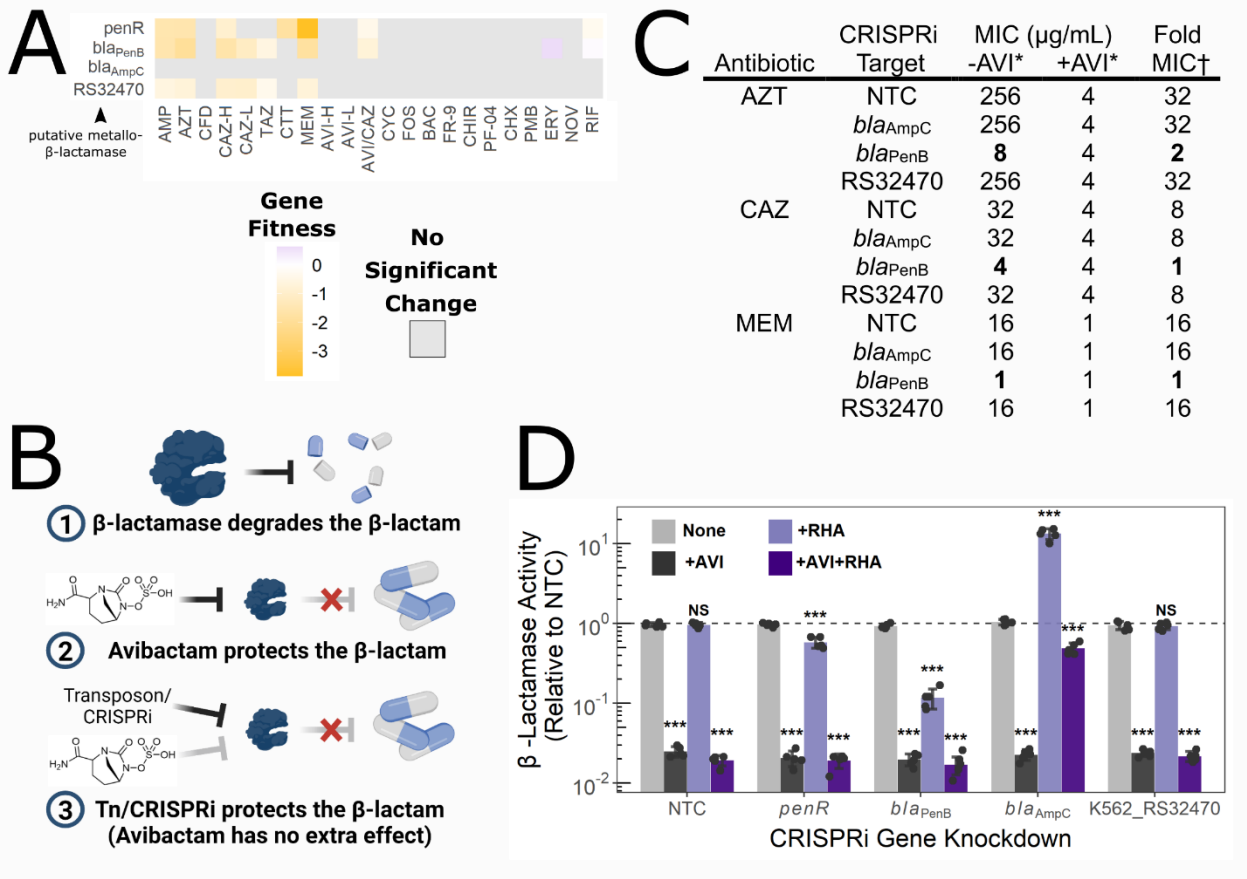

Antibiotic	CRISPRi Target	MIC (μg/mL) -AVI*	MIC (μg/mL) +AVI*	Fold MIC†
AZT	NTC	256	4	32
	bla$_{AmpC}$	256	4	32
	bla$_{PenB}$	**8**	4	**2**
	RS32470	256	4	32
CAZ	NTC	32	4	8
	bla$_{AmpC}$	32	4	8
	bla$_{PenB}$	**4**	4	**1**
	RS32470	32	4	8
MEM	NTC	16	1	16
	bla$_{AmpC}$	16	1	16
	bla$_{PenB}$	**1**	1	**1**
	RS32470	16	1	16

Figure 6. PenB is the predominant β-lactamase in K56-2 and is inhibited by AVI. A) Gene fitness scores relative to the DMSO control of β-lactamase and regulatory genes. B) Rationale for identifying targets of AVI. If a target is disrupted with a transposon or repressed with CRISPRi there will be no change in β-lactam MIC when AVI is added. C) MIC values of K56-2::dCas9 harbouring plasmids expressing a non-targeting sgRNA control (NTC) or an sgRNA targeting the indicated genes. MIC values are medians of three biological replicates, with bold indicating change versus the NTC. † Fold MIC is the ratio of the MIC -AVI to the MIC +AVI. * AVI kept constant at 8 μg/mL. D) Nitrocefin hydrolysis assay of lysate from CRISPRi mutants grown in the indicated conditions. Values are means of five biological replicates, with the dashed line indicating no difference vs. the NTC. Significance was determined by an unpaired two-tailed t-test to the NTC grown without rhamnose or AVI using Bonferroni's correction. *** $P < 0.001$

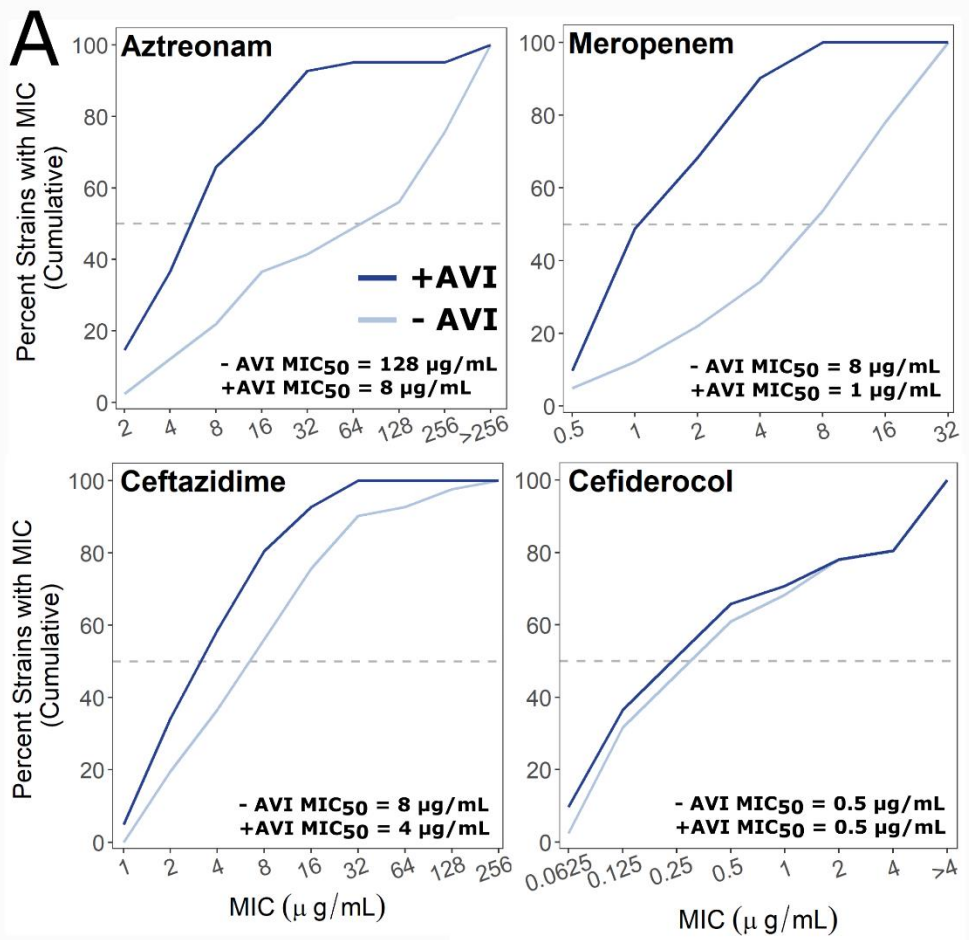

B

	AZT		MEM		CAZ		CFD	
	-AVI	+AVI	-AVI	+AVI	-AVI	+AVI	-AVI	+AVI
Resistant/Total Isolates	24/41	2/41	9/41	0/41	4/41	0/41	8/41	8/41
(% Resistant)	(59%)	(5%)	(22%)	(0%)	(10%)	(0%)	(20%)	(20%)

Figure 7. AVI strongly potentiates AZT and MEM in Bcc clinical isolates. A) Percent cumulative growth inhibition of 41 Bcc clinical isolates with or without AVI. The dashed line indicates the MIC_{50}, the concentration at which 50% of the isolates were inhibited. Data for panels A and B were summarized from Table S3. B) Resistance to AZT, MEM, CAZ, and CFD with or without 8 µg/mL AVI. CLSI resistance breakpoints for the Bcc: MEM ≥ 16 µg/mL; CAZ ≥ 32 µg/mL. CLSI resistance breakpoints for *P. aeruginosa* were used for AZT (≥ 32 µg/mL) and CFD (> 4 µg/mL) as none exist for the Bcc.

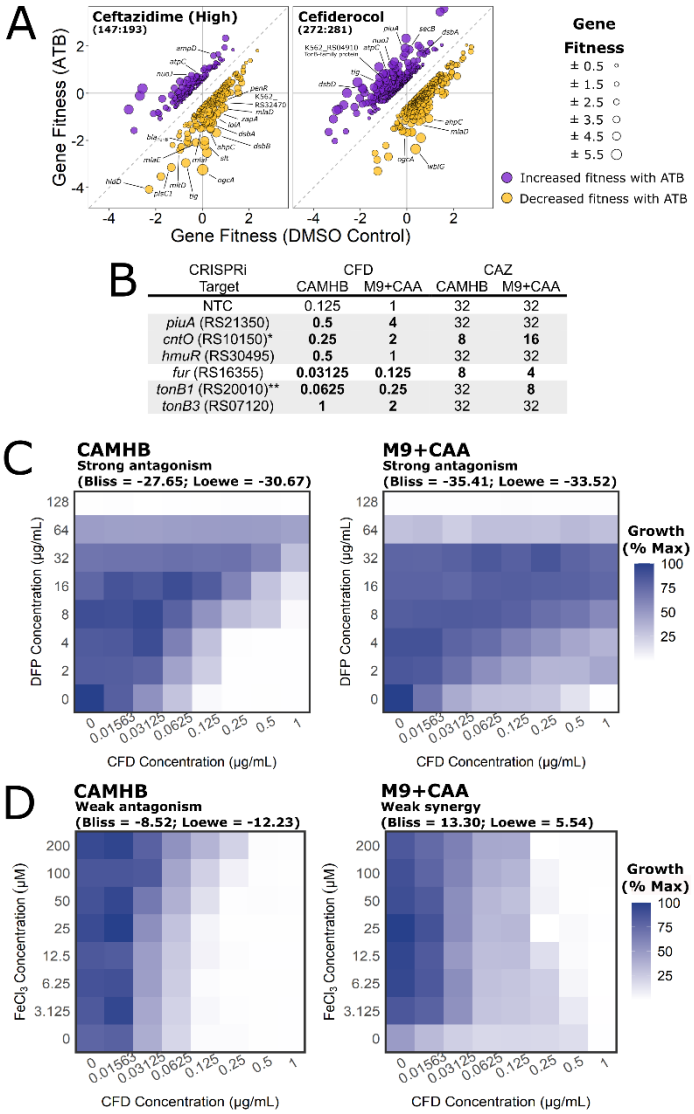

CRISPRi Target	CFD CAMHB	CFD M9+CAA	CAZ CAMHB	CAZ M9+CAA
NTC	0.125	1	32	32
piuA (RS21350)	**0.5**	**4**	32	32
cntO (RS10150)*	**0.25**	**2**	**8**	**16**
hmuR (RS30495)	**0.5**	1	32	32
fur (RS16355)	**0.03125**	**0.125**	**8**	**4**
tonB1 (RS20010)**	**0.0625**	**0.25**	32	**8**
tonB3 (RS07120)	**1**	**2**	32	32

Figure 8. CFD uptake in K56-2 is strongly dependent on growth medium iron concentration. A) Gene fitness profiles of CAZ and CFD. The points are coloured based on positive (increased fitness; purple) or negative (decreased fitness; gold) interactions. All fitness profiles are found in Figure S5. B) Susceptibility of CRISPRi mutants in genes associated with iron uptake to cefiderocol and ceftazidime in CAMHB and M9+CAA. MIC values (µg/mL) presented are medians of at least four biological replicates in the presence of 0.5% rhamnose. Bold indicates at least 2-fold difference from the NTC. Gene names are assigned by homology, if known, or else the locus tag is given (preceded by K562_). *K562_RS10150 was assigned as a strong homologue to *P. aeruginosa* PAO1 *cntO* but failed reciprocal best-hit BLAST. ** *tonB* paralogues are assigned based on similarity to the *P. aeruginosa* PAO1 *tonB1*. C) Growth of K56-2 in a 2-dimensional antibiotic gradient of CFD and deferiprone in CAMHB and M9+CAA. D) The same as for panel B, but with CFD and $FeCl_3$. Values are normalized to the OD_{600} of the well with the most growth. Interactions were assessed and interpreted with SynergyFinder.

References (only cited in figure legends)

1. Bernier SP, Son S, Surette MG. The Mla pathway plays an essential role in the intrinsic resistance of *Burkholderia cepacia* complex species to antimicrobials and host innate components. J Bacteriol. 2018;200: e00156-18. doi:10.1128/JB.00156-18

2. Powers MJ, Simpson BW, Trent MS. The Mla pathway in *Acinetobacter baumannii* has no demonstrable role in anterograde lipid transport. eLife. 2020;9: e56571. doi:10.7554/eLife.56571

3. Egan AJF, Errington J, Vollmer W. Regulation of peptidoglycan synthesis and remodelling. Nat Rev Microbiol. 2020;18: 446–460. doi:10.1038/s41579-020-0366-3

4. Manat G, Roure S, Auger R, Bouhss A, Barreteau H, Mengin-Lecreulx D, et al. Deciphering the metabolism of undecaprenyl-phosphate: the bacterial cell-wall unit carrier at the membrane frontier. Microb Drug Resist. 2014;20: 199–214. doi:10.1089/mdr.2014.0035

5. Mohamed YF, Scott NE, Molinaro A, Creuzenet C, Ortega X, Lertmemongkolchai G, et al. A general protein O-glycosylation machinery conserved in *Burkholderia* species improves bacterial fitness and elicits glycan immunogenicity in humans. J Biol Chem. 2019;294: 13248–13268. doi:10.1074/jbc.RA119.009671

6. Valvano MA. Chapter 4 - Genetics and biosynthesis of lipopolysaccharide. In: Tang Y-W, Sussman M, Liu D, Poxton I, Schwartzman J, editors. Molecular medical microbiology (Second Edition). Boston: Academic Press; 2015. pp. 55–89. doi:10.1016/B978-0-12-397169-2.00004-4

7. Ortega X, Silipo A, Saldías MS, Bates CC, Molinaro A, Valvano MA. Biosynthesis and structure of the *Burkholderia cenocepacia* K56-2 lipopolysaccharide core oligosaccharide: truncation of the core oligosaccharide leads to increased binding and sensitivity to polymyxin B. J Biol Chem. 2009;284: 21738–21751. doi:10.1074/jbc.M109.008532